Theory of coupled translational-rotational glassy dynamics in dense fluids of uniaxial particles

Rui Zhang and Kenneth S. Schweizer*
Department of Materials Science and Frederick Seitz Materials Research Laboratory, University of Illinois, 1304 West Green Street, Urbana, Illinois 61801, USA
(Received 3 April 2009; published 24 July 2009)

The naïve mode coupling theory (NMCT) for ideal kinetic arrest and the nonlinear Langevin equation theory of activated single-particle barrier hopping dynamics are generalized to treat the coupled center-of-mass (CM) translational and rotational motions of uniaxial hard objects in the glassy fluid regime. The key dynamical variables are the time-dependent displacements of the particle center-of-mass and orientational angle. The NMCT predicts a kinetic arrest diagram with three dynamical states: ergodic fluid, plastic glass, and fully nonergodic double glass, the boundaries of which meet at a "triple point" corresponding to a most difficult to vitrify diatomic of aspect ratio ~1.43. The relative roles of rotation and translation in determining ideal kinetic arrest are explored by examining three limits of the theory corresponding to nonrotating, pure rotation, and rotationally ergodic models. The ideal kinetic arrest boundaries represent a crossover to activated dynamics described by two coupled stochastic nonlinear Langevin equations for translational and rotational motions. The fundamental quantity is a dynamic free-energy surface, which for small aspect ratios in the high-volume fraction regime exhibits two saddle points reflecting a two-step activated dynamics where relatively rapid rotational dynamics coexists with slower CM translational motions. For large-enough aspect ratios, the dynamic free-energy surface has one saddle point which corresponds to a system-specific coordinated translation-rotation motion. The entropic barriers as a function of the relative amount of rotation versus translation are determined.

DOI: 10.1103/PhysRevE.80.011502 PACS number(s): 64.70.Q−, 82.70.Dd, 83.80.Hj

I. INTRODUCTION

Glassy dynamics and kinetic structural arrest are of broad interest and relevance in both thermal liquids and colloidal and nanoparticle suspensions [1,2]. Despite intense theoretical and simulation activities in this area over the last decade or two, with few exceptions, the focus has been on simple spherical particle model fluids. In reality, most thermal glass-forming materials involve more complex elementary constituents, the most generic aspect of which is anisotropic particle shape. A similar diversity exists at the nanometer and colloidal scales where large aspect ratio disks, rods, ellipsoids, and spherocylinders are classic nonspherical objects [3,4]. Recent advances in materials science [5–7] have led to the creation of a vast array of nonspherical colloids and nanoparticles, perhaps the simplest of which is a "dicolloid" which is the analog of a homonuclear diatomic molecule of variable length-to-width ratio.

Microscopic ideal mode coupling theory (MCT) [8,9] studies of dense fluids of hard-core ellipsoids [10] and homonuclear diatomics [11] have been recently performed. Many interesting results have emerged, including the prediction of a plastic glass state and a nonmonotonic dependence of the ideal glass transition volume fraction and transport coefficients on particle aspect ratio. These predictions have been partially confirmed via computer simulation of related models in the dynamic crossover regime [12–15]. However, the strict MCT nonergodicity transition is known to be an artifact of neglecting nonperturbative activated barrier hopping processes, and simulations have found evidence of the qualitative importance of rotational hopping even in the dynamical crossover regime [13].

One of us and his collaborators recently developed and widely applied a first-principles microscopic theory of strongly activated single-particle center-of-mass translational dynamics in fluids and suspensions of hard spheres [16,17] and uniaxial objects [18]. Our starting point is the simplified naïve mode coupling theory (NMCT) [16,19] as restricted to center-of-mass (CM) translational motions [18]. Despite the limited number of questions that CM-NMCT addresses, it has successfully treated within a mathematically and conceptually simple framework ideal kinetic vitrification for hard spheres [16,17], hard linear molecules [18], re-entrant glass-fluid-gel melting in dense attractive sphere fluids [20], and partial and full localizations in binary mixtures of hard and sticky spheres [21]. Beyond MCT nonlinear Langevin equation (NLE) theory [16,17,22] (and simulation [23]) predicts that MCT-like critical power-law behavior emerges as a crossover phenomenon associated with activated hopping over relatively low barriers. Specifically, the variation with volume fraction of the relaxation time and self-diffusion constant in the beginning stages of the barrier hopping regime can be empirically fit by a critical power law form despite being beyond the ideal MCT arrest transition [16,17]. Connections with jamming in granular media [24,25] have also been made [18,26]. However, explicit treatment of rotational dynamics, both at the NMCT and beyond levels, has not been achieved.

The goal of the present paper is to generalize the NMCT and nonlinear Langevin equation theories for nonspherical particles to explicitly treat orientational dynamics. Section II presents the approach at the NMCT level and three special limits are examined in Sec. III. Numerical results for the ideal kinetic arrest phase diagram, localization properties,

*Corresponding author; kschweiz@illinois.edu

and nonergodicity factors of hard diatomics are given in Sec. IV. Extension of the theory to treat activated dynamics is given in Sec. V and sample calculations of dynamical free-energy surfaces and entropic barriers as a function of aspect ratio and volume fraction are presented. The paper concludes in Sec. VI with a summary and future outlook. Appendix A derives the uniaxial particle dynamic structure factor, and a detailed analysis of the vertices for interparticle forces and torques is given in Appendix B.

II. NAÏVE MODE COUPLING THEORY

We consider one-component fluids of rigid uniaxial objects described as a linear chain of N bonded interaction sites (diameter D) that interact via pair decomposable excluded volume forces. The dynamical theory can be formulated for this general class of objects. However, in this initial work, we focus on the simplest and highest symmetry realization: a homonuclear diatomic of $N=2$ identical sites separated by a bond length b corresponding to an aspect ratio of $L/D=1+(b/D)$. The original generalization of NMCT to nonspherical particles invoked an *a priori* mapping to a reduced center-of-mass description which ignored orientational dynamics [18]. To set the stage for our theory which removes this limitation, the CM theory is derived from a more general site perspective.

A. Center-of-mass naïve mode coupling theory

The central quantity in NMCT is the time-correlation function matrix of forces [18] felt by sites i and j on a tagged diatomic due to the surrounding molecules, $K_{ij}(t) \equiv \langle \mathbf{f}_i(0)\cdot\mathbf{f}_j(t)\rangle$. Based on standard MCT projection and factorization approximations, the real forces are replaced by an effective force between site i on the tagged diatomic and site k on a different molecule given by $-k_BT\, dC_{ik}(r)/dr$, where k_BT is the thermal energy and C_{ik} is the site-site direct correlation function. In a Fourier-resolved representation, $K_{ij}(t)$ involves the quantity $q^2[\underset{\sim}{C}(q)\underset{\sim}{S}(q,t)\underset{\sim}{C}(q)]_{ij}\omega_{ij}(q,t)$, where $\omega_{ij}(q,t)$ and $S_{ij}(q,t)$ are the corresponding matrix elements of the dimensionless single molecule and collective density-fluctuation dynamic structure factors, respectively. The force correlations temporally decay in a parallel fashion via collective relaxation of the surrounding media as quantified by $\underset{\sim}{S}(q,t)$ and via tagged particle motion as quantified by $\underset{\sim}{\omega}(q,t)$. Assembling these theoretical elements, one obtains [18,21]

$$\langle \mathbf{f}_i(0)\cdot\mathbf{f}_j(t)\rangle = \frac{1}{3\beta^2}\int \frac{d\mathbf{q}}{(2\pi)^3}\rho q^2 \sum_{k,l}^{2} \omega_{ij}(q)C_{ik}(q)C_{jl}(q)S_{kl}(q)\Gamma_S^{(ij)}(q,t)\Gamma_C^{(kl)}(q,t)$$
$$= \frac{1}{3\beta^2}\int \frac{d\mathbf{q}}{(2\pi)^3}\rho q^2 C_{ss}^2(q)\omega_{ij}(q)\Gamma_S^{(ij)}(q,t)\sum_{k,l}^{2} S_{kl}(q)\Gamma_C^{(kl)}(q,t), \quad (1)$$

where ρ is the molecular number density, the second line has used the symmetry relation for a homonuclear diatomic, $C_{ij}(q)=C_{ss}(q)$, where "ss" refers to site-site, and normalized (at $t=0$) single molecule and collective dynamic "propagators" are defined as

$$\Gamma_S^{(ij)}(q,t) = \omega_{ij}(q,t)/\omega_{ij}(q), \quad (2)$$

$$\Gamma_C^{(kl)}(q,t) = S_{kl}(q,t)/S_{kl}(q). \quad (3)$$

The single molecule dynamic structure factor matrix is

$$\omega_{ij}(q,t) = \langle e^{i\mathbf{q}\cdot[\mathbf{r}_i(t)-\mathbf{r}_j(0)]}\rangle, \quad (4)$$

where $\omega_{jj}(q)=1$ and $\omega_{12}(q)=\sin(qb)/qb$.

We now transform from the site representation to the center-of-mass and orientation representation using $\vec{r}_1=\vec{R}_{\mathrm{CM}}+\vec{b}/2$ and $\vec{r}_2=\vec{R}_{\mathrm{CM}}-\vec{b}/2$ and rewrite Eq. (4) as

$$\Gamma_S^{(ij)}(q,t) = \langle e^{i\vec{q}\cdot[\vec{R}_{\mathrm{CM}}(t)-\vec{R}_{\mathrm{CM}}(0)]}e^{i\vec{q}\cdot[(-1)^{i+1}\vec{b}(t)+(-1)^{j}\vec{b}(0)]/2}\rangle/\omega_{ij}(q). \quad (5)$$

Equation (5) makes explicit the fact that both CM translational and rotational motions contribute to the temporal decay of the single molecule site-site density correlations. To recover the original CM version of NMCT [18], relaxation is assumed to occur solely via center-of-mass translation

$$\Gamma_S^{(ij)}(q,t) \approx \langle e^{i\vec{q}\cdot[\vec{R}_{\mathrm{CM}}(t)-\vec{R}_{\mathrm{CM}}(0)]}\rangle \equiv \Gamma_S^{\mathrm{CM}}(q,t), \quad (6)$$

$$\Gamma_C^{(ij)}(q,t) \approx \Gamma_C^{\mathrm{CM}}(q,t), \quad (7)$$

which follow from Eq. (5) if $\vec{b}(t)=\vec{b}(0)$, i.e., molecules do not rotate. Equations (6) and (7) can alternatively, and more generally, be viewed as a special case of the "dynamic site equivalency" approximation that is utilized in Sec. II B to treat rotations. Using Eqs. (6) and (7) in Eq. (1) yields

$$\langle \mathbf{f}_i(0)\cdot\mathbf{f}_j(t)\rangle = \frac{1}{3\beta^2}\int \frac{d\mathbf{q}}{(2\pi)^3}\rho_s S_{ss}(q)q^2C_{ss}^2(q)\omega_{ij}(q)\Gamma_S^{\mathrm{CM}}(q,t)\Gamma_C^{\mathrm{CM}}(q,t), \quad (8)$$

where the site-site level collective static structure factor is

$$S_{ss}(q) \equiv N^{-1} \sum_{i,j=1}^{N} S_{ij}(q). \tag{9}$$

Since only CM motions are retained, the sole relevant force-force time-correlation function is

$$K_{\mathrm{CM}}(t) \equiv \sum_{i,j=1}^{N} \langle \mathbf{f}_i(0) \cdot \mathbf{f}_j(t) \rangle = \frac{N}{3\beta^2} \int \frac{d\mathbf{q}}{(2\pi)^3} \rho_s S_{ss}(q) q^2 C_{ss}^2(q) \omega_{ss}(q) \times \Gamma_S^{\mathrm{CM}}(q,t) \Gamma_C^{\mathrm{CM}}(q,t), \tag{10}$$

where the total single molecule static structure factor of the diatomic is

$$\omega_{ss}(q) \equiv N^{-1} \sum_{i,j=1}^{N} \omega_{ij}(q) = 1 + \frac{\sin(qb)}{qb}. \tag{11}$$

Equation (10) can be explicitly rewritten in the purely CM dynamical theory form by first recalling the reference interaction site model (RISM) integral equation in Fourier space for site-site equilibrium pair correlations of a fluid composed of identical interaction sites [27,28]

$$h_{ss}(k) = \omega_{ss}(k) C_{ss}(k) \omega_{ss}(k) + \rho_s \omega_{ss}(k) C_{ss}(k) h_{ss}(k), \tag{12}$$

$$S_{ss}(k) \equiv \omega_{ss}(k) + \rho_s h_{ss}(k) = \frac{1}{\omega_{ss}^{-1}(k) - \rho_s C_{ss}(k)}, \tag{13}$$

where $\rho_s = N\rho$ is the site number density and $h_{ss}(k)$ is the Fourier transform of the intermolecular site-site total correlation function, $h_{ss}(r) = g_{ss}(r) - 1$. For hard-core interactions, the site-site Percus-Yevick (PY) closure is [27]

$$C_{ss}(r) = 0, \quad r > D. \tag{14}$$

The CM and site level total structure factors are related by adopting the "rigid particle" approximation [29] discussed in depth previously [18]

$$S_{ss}(k) \cong \omega_{ss}(k) S_{\mathrm{CM}}(k). \tag{15}$$

At the CM level, the Ornstein-Zernike relation of an atomic liquid applies [30]

$$S_{\mathrm{CM}}(k) = 1 + \rho h_{\mathrm{CM}}(k) = \frac{1}{1 - \rho C_{\mathrm{CM}}(k)}. \tag{16}$$

Comparing Eqs. (13) and (14), one has

$$C_{\mathrm{CM}}(k) = N \omega_{ss}(k) C_{ss}(k), \tag{17}$$

$$h_{\mathrm{CM}}(k) \equiv \frac{N}{\omega_{ss}(k)} h_{ss}(k), \tag{18}$$

which are equivalent statements of the rigid particle mapping. Combining Eqs. (15)–(17) yields the CM-NMCT theory for the force time-correlation function

$$K_{\mathrm{CM}}(t) = \frac{1}{3\beta^2} \int \frac{d\mathbf{q}}{(2\pi)^3} \rho S_{\mathrm{CM}}(q) q^2 C_{\mathrm{CM}}^2(q) \Gamma_S^{\mathrm{CM}}(q,t) \Gamma_C^{\mathrm{CM}}(q,t). \tag{19}$$

For liquids, $\Gamma_S^{\mathrm{CM}}(q,t)$ and $\Gamma_C^{\mathrm{CM}}(q,t) \to 0$ as $t \to \infty$, but for ideal solids, these propagators are nonergodicity parameters or Debye-Waller (DW) factors. Within NMCT, they are taken to be of an Einstein oscillator (harmonic solid) form [16,18,19]

$$\Gamma_S(q, t \to \infty) = \exp(-q^2 r_{loc}^2/6), \tag{20}$$

$$\Gamma_C(q, t \to \infty) = \exp[-q^2 r_{loc}^2/6 S_{\mathrm{CM}}(q)], \tag{21}$$

where r_{loc} is the CM localization length and the classic de Gennes narrowing correlation of the relaxation rate of collective density fluctuations with the inverse of the structure factor [16,30] is included in Eq. (21). This correction to a literal Vineyard approximation [16,19,30] [$\Gamma_S^{\mathrm{CM}}(q,t) \approx \Gamma_C^{\mathrm{CM}}(q,t)$] is quantitatively important and can be motivated in several ways. The most transparent follows from a short-time analysis of $S_{\mathrm{CM}}(q,t)$ in the overdamped limit where [21,31]

$$\frac{d}{dt} S_{\mathrm{CM}}(q,t) = -q^2 D_0 S_{\mathrm{CM}}^{-1}(q) S_{\mathrm{CM}}(q,t) \tag{22}$$

and D_0 is the short-time self-diffusion constant. Solving for $S_{\mathrm{CM}}(q,t)$ yields

$$S_{\mathrm{CM}}(q,t) = S_{\mathrm{CM}}(q) e^{-q^2 D_0 t / S_{\mathrm{CM}}(q)} = S_{\mathrm{CM}}(q) e^{-q^2 \langle r_{\mathrm{CM}}^2(t) \rangle / 6 S_{\mathrm{CM}}(q)}. \tag{23}$$

The second equality follows from the underlying assumption of short-time Fickian self-diffusion. Equation (23) is relevant to the ideal glass problem since particle localization occurs on short length scales. This motivates the identification of $S_{\mathrm{CM}}(q, t \to \infty)$ in NMCT via $\langle r_{\mathrm{CM}}^2(t \to \infty) \rangle \equiv r_{loc}^2$ (or equivalently the replacement $6D_0 t \to r_{loc}^2$), thereby yielding Eq. (21). This arrested short-time dynamics analysis is an alternative motivation for the Gaussian Debye-Waller factors of Eqs. (20) and (21).

Using Eqs. (20) and (21) in Eq. (19), the localization length can be self-consistently computed which is equivalent to enforcing an equipartition relation given by [16,18,21]

$$\beta K_{\mathrm{CM}}(t \to \infty; r_{loc}) r_{loc}^2/2 = 3 k_B T/2. \tag{24}$$

The NMCT theory self-consistency equation for the localization length is then

$$r_{loc}^{-2} = \frac{1}{9} \int \frac{d\vec{q}}{(2\pi)^3} \rho q^2 C_{\mathrm{CM}}^2(q) S_{\mathrm{CM}}(q) e^{-(q^2 r_{loc}^2/6)[1 + S_{\mathrm{CM}}^{-1}(q)]}, \tag{25}$$

which is identical in form to that for an atomic (sphere) fluid [16].

B. NMCT for rotating and translating diatomics

The nature of rotational localization, and the possibility of a partial localization transition into an orientationally ergodic

but translationally arrested "plastic glass" state, is not addressed by the CM-NMCT. The starting point for generalization is Eq. (1) for the site-level force time-correlation function matrix. Knowledge of the single molecule and collective density-fluctuation matrix propagators, and how they are related to CM and rotational motions, is the source of the high technical complexity in extending MCT for spheres to nonspherical objects within either the site [11] or Euler rigid body formulations [10]. To render this aspect tractable in a physically transparent and tractable manner that allows extension to treat barrier hopping, we propose the "dynamic site equivalency" (DSE) approximation. For the single molecule dynamic structure factor matrix, this corresponds to approximating all matrix elements by the average

$$\Gamma_S^{(ij)}(q,t) \approx \Gamma_S^{ss}(q,t) \equiv \frac{\omega_{ss}(q,t)}{\omega_{ss}(q)}. \tag{26}$$

The physical idea is that the long-time site level dynamics is of a "slaved" nature due to the rigid body nature of translations and rotations. Recall that NMCT approximates propagators by their short-time form, which is then mapped onto an Einstein description of an ideal solid. For a uniaxial object, the propagator in Eq. (26) can be exactly determined under short-time dynamical conditions as described in Appendix A. The result is

$$\Gamma_S^{ss}(q,t) = 2\omega_{ss}^{-1}(q)\sum_{l=0}^{\infty} j_{2l}^2(qb/2)(4l+1) \times \exp\{-[q^2 D_T + 2l(2l+1)D_R]t\}, \tag{27}$$

where D_T and D_R are the short-time CM and rotational diffusion constants, respectively, $j_{2l}(x)$ is the spherical Bessel function of order $2l$, and an infinite summation over angular-momentum states is required. For *fixed* wave vector, single molecule density fluctuations decay in a parallel and multiplicative manner via CM and rotational motions. Such a Fourier space description of the self-dynamic structure factor is often used for dense molecular fluids in the normal liquid regime [32].

To proceed, a specific description of the rotational degree of freedom is required. For a uniaxial object, one angle fully describes this motion. The classic Debye approach [33,34] appropriate for continuous orientational diffusion is based on an angle $\psi(t)$ defined as $\psi(t)=\cos^{-1}[\vec{u}(0)\cdot\vec{u}(t)]$, where the unit vector $\vec{u}(t) \equiv \vec{b}(t)/b$. In this formulation, $\psi(t)$ is bounded between zero and π, corresponding to motion of the unit vector on the surface of a sphere, and hence is not sensitive to the full particle rotations. As discussed by others [34–36], this description is not appropriate for glassy (intermittent) dynamics and a rotational diffusion constant cannot be defined based on the usual Fickian formula. Rather, an "Einstein formulation" is required corresponding to an *unbounded*, cumulative angular *displacement* degree of freedom given by [35,36]

$$\theta(t) \equiv |\vec{\theta}(t)|,$$

$$\vec{\theta}(t) = \int_0^t dt' \vec{\omega}(t'), \tag{28}$$

where $\vec{\omega}$ is the angular velocity. This cumulative angular displacement relative to the initial ($t=0$) orientation allows a rotational trajectory to be defined which, in analogy with translational motion, results in a rotational mean-square displacement that obeys the Fickian relation at long times

$$\lim_{t\to\infty}\langle\theta^2(t)\rangle = 4D_R t. \tag{29}$$

The beyond MCT nonlinear Langevin equation theory proposed in Sec. IV for the orientational dynamics is formulated in terms of this cumulative angular displacement variable. For small times and angular displacement, the Debye and Einstein formulations are identical corresponding to

$$\langle\theta^2(t)\rangle = 4D_R t, \tag{30}$$

$$\langle(\vec{R}_{\rm CM}(t) - \vec{R}_{\rm CM}(0))^2\rangle = 6D_T t. \tag{31}$$

For NMCT based on a harmonic Einstein solid picture, Eqs. (30) and (31) imply, in analogy with the sphere analysis, that $(6D_T t\to\infty) \equiv r_{loc}^2$ and $(4D_R t\to\infty) \equiv \theta_{loc}^2$ (radians) in Eq. (27)

$$\Gamma_S^{(ij)}(q,t\to\infty) \approx \Gamma_S^{(ss)}(q,t\to\infty) = 2\left[1+\frac{\sin(qb)}{qb}\right]^{-1}\left\{\sum_{l=0}^{\infty} j_{2l}^2(qb/2)(4l+1) \times \exp[-l(2l+1)\theta_{loc}^2/2]\right\} \times \exp(-q^2 r_{loc}^2/6), \tag{32}$$

where r_{loc} and θ_{loc} are the CM localization length and localization angle. The collective density-fluctuation propagator is treated in the same DSE spirit

$$\Gamma_C^{(ij)}(q,t) \approx \Gamma_C^{ss}(q,t) \equiv \frac{S_{ss}(q,t)}{S_{ss}(q)}, \tag{33}$$

and the de Gennes–corrected Vineyard approximation is again adopted to relate single and many particle dynamic fluctuations

$$\Gamma_C^{(ij)}(q,t\to\infty) \approx 2\left[1+\frac{\sin(qb)}{qb}\right]^{-1}\left\{\sum_{l=0}^{\infty} j_{2l}^2(qb/2)(4l+1) \times \exp[-l(2l+1)\theta_{loc}^2/2g_2]\right\} \times \exp[-q^2 r_{loc}^2 S_{\rm CM}^{-1}(q)/6]. \tag{34}$$

By analogy with the treatment of translations, an orientational de Gennes–like correction is employed in Eq. (34) via the second-rank orientational correlation factor, g_2, associated with many molecule static angular correlations and defined as [37]

$$g_2 \equiv 1 + n^{-1} \sum_{i \neq j=1}^{n} \langle P_2[\vec{u}_i \cdot \vec{u}_j] \rangle, \tag{35}$$

where n is the number of molecules, P_2 is the second Legendre polynomial, and $\vec{u}_j$ is a unit vector that defines the orientation of linear molecule j. The single-particle reorientation time, $\tau_{S,R}$, and collective reorientation time, $\tau_{C,R}$, are related as [37] $\tau_{C,R} \simeq g_2 \tau_{S,R}$. Equation (34) assumes the reorientation time is inversely proportional to the rotational diffusion coefficient and hence $D_R \to D_R / g_2$. In general, g_2 is modestly larger than unity ($\sim 1.1-2$) for nonspherical molecular liquids [38]. For our system, g_2 depends on diatomic aspect ratio and is expected to increase with particle elongation and volume fraction. However, there is no quantitative knowledge of g_2 for hard diatomics of the aspect ratios and very high volume fractions of present interest. Fortunately, this correction has little effect since it is not large compared to unity and is a pure numerical factor, not a wave-vector–dependent correction. In what follows, $g_2 = 1$ unless stated otherwise.

Two coupled self-consistent equations for the localization length and angle can now be derived within the NMCT framework. In the Einstein solid description, $K_{\mathrm{CM}} \equiv \beta \langle \vec{F}_{\mathrm{CM}}(0) \cdot \vec{F}_{\mathrm{CM}}(t \to \infty) \rangle$ is an effective spring constant for CM displacement and $K_{ROT} \equiv \beta \langle \vec{T}(0) \cdot \vec{T}(t \to \infty) \rangle$ is an effective spring constant for rotation. Here, $\vec{F}_{\mathrm{CM}} = \vec{f}_1 + \vec{f}_2$ is the total force on the diatomic CM and $\vec{T} = (b/2)\vec{u} \times (\vec{f}_1 - \vec{f}_2)$ is the total torque where $\vec{u}$ is the unit vector along the diatomic axis. The NMCT self-consistency equations are of a classical equipartition relation form

$$K_{\mathrm{CM}} r_{loc}^2 / 2 = 3 k_B T / 2, \tag{36}$$

$$K_{ROT} \theta_{loc}^2 / 2 = k_B T. \tag{37}$$

Combining Eqs. (1), (32), (34), (36), and (37) yields two coupled equations for r_{loc} and θ_{loc},

$$\begin{aligned} r_{loc}^{-2} &= \frac{2}{9\pi^2} \int_0^\infty dq \rho q^4 C_{\mathrm{CM}}^2(q) S_{\mathrm{CM}}(q) [1 + \sin(qb)/qb]^{-2} \\ &\quad \times \exp\{-q^2 [1 + S_{\mathrm{CM}}^{-1}(q)] r_{loc}^2 / 6\} \\ &\quad \times \left\{ \sum_{l=0}^{\infty} j_{2l}^2(qb/2)(4l+1) \exp[-l(2l+1)\theta_{loc}^2/2] \right\}^2 \\ &\equiv \int_0^\infty dq 4 [1 + \sin(qb)/qb]^{-2} V_{\mathrm{CM}}(q) \\ &\quad \times \exp\{-q^2 [1 + S_{\mathrm{CM}}^{-1}(q)] r_{loc}^2 / 6\} \\ &\quad \times \left\{ \sum_{l=0}^{\infty} j_{2l}^2(qb/2)(4l+1) \exp[-l(2l+1)\theta_{loc}^2/2] \right\}^2, \end{aligned} \tag{38}$$

$$\begin{aligned} \theta_{loc}^{-2} &= \frac{b^2}{12\pi^2} \exp(-\theta_{loc}^2/2) \int_0^\infty dq \rho q^4 C_{\mathrm{CM}}^2(q) S_{\mathrm{CM}}(q) \\ &\quad \times [1 - \sin(qb)/qb][1 + \sin(qb)/qb]^{-3} \\ &\quad \times \exp\{-q^2 [1 + S_{\mathrm{CM}}^{-1}(q)] r_{loc}^2 / 6\} \\ &\quad \times \left\{ \sum_{l=0}^{\infty} j_{2l}^2(qb/2)(4l+1) \exp[-l(2l+1)\theta_{loc}^2/2] \right\}^2. \end{aligned} \tag{39}$$

Equations (38) and (39) constitute the new naïve MCT. A center-of-mass "vertex" [18,26] is defined in the second line of Eq. (38) which corresponds to the integrand on the right-hand side of the equation when $r_{loc} = \theta_{loc} = 0$. The vertex represents a Fourier-resolved effective mean-square force exerted by the fluid on a tagged molecule center of mass. Note that CM and rotational localization, as encoded in the Debye-Waller factors, are now coupled via the wave-vector integration. In Appendix B, a detailed analysis of the wave-vector scaling of the force and torque vertices is presented which provides a deeper understanding of the dynamical role of correlations on different length scales. Here we simply note that the limiting behaviors of the Bessel function contributions are $j_{2l}(qb) \propto (qb)^{2l}$ as $q \to 0$ and $j_{2l}(qb) \propto (qb)^{-1}$ for all l as $qb \to \infty$. The presence of the $l=0$ contribution in Eqs. (38) and (39) implies the ergodic rotational state ($\theta_{loc} \to \infty$) differs from the simpler CM description. The latter is recovered from Eq. (38) under the nonrotating condition ($\theta_{loc} = 0$) using the sum-rule formula for spherical Bessel functions.

III. LIMITING CASES

Before implementing the new NMCT, we consider three limiting cases which provide physical insight about the dominant relaxation channel.

A. Effectively frozen rotation

Consider an isotropic fluid of globally randomly oriented diatomics. Now imagine the molecules dynamically translate but do not rotate. This corresponds to $\theta_{loc} = 0$ in Eq. (38), which then reduces to the CM version of NMCT [18] of Eq. (25). Although not literally true, this simplification is relevant (as shown below) for small aspect ratio diatomics due to the dominance of high wave-vector force correlations. Indeed, if one sets $\theta_{loc} = 0$ in Eq. (38), then the amplitude of the vertex in Eq. (38) is *independent* of q at high wave vectors [18]. Alternatively, the effectively frozen rotation limit corresponds to CM translation being far more effective at relaxing intermolecular forces than rotational motions. Such a simplification must overpredict the tendency to localize since rotational motions provide an additional mechanism for escaping confining forces and torques.

B. Effectively ergodic rotation

The opposite limit of ergodic rotation assumes that rotational motion is fluidlike ($\theta_{loc} = \infty$). This limit is expected to

be relevant at low aspect ratios where only the CM is localized and the system is in a plastic glass state. Setting $\theta_{loc}=\infty$ in Eq. (38), one obtains

$$r_{loc}^{-2}=\frac{32}{9\pi^2}\int_0^\infty dq\rho q^4 C_{\rm CM}^2(q)S_{\rm CM}(q)\frac{\sin^4(qb/2)}{(qb)^4}\times\left[1+\frac{\sin(qb)}{qb}\right]^{-2}\exp\{-q^2[1+S_{\rm CM}^{-1}(q)]r_{loc}^2/6\}. \quad (40)$$

Unlike the frozen rotation limit, which can never be exact since $\theta_{loc}=0$ does not satisfy Eq. (39), ergodic rotation can be exact for a plastic glass. The wave-vector scaling of the vertex in Eq. (40) is also different than the frozen rotation (CM-NMCT) case [18]; it grows as $\sim q^4$ at small wave vectors and decays to zero as $\sim 1/q^4$ in the high q limit. Hence, the nonmonotonic dependence of the vertex on q implies the existence of a characteristic intermediate wave vector and hence length scale.

C. Effectively frozen center-of-mass

In analogy with the frozen rotation model, one can consider the frozen CM limit corresponding to molecules starting in equilibrated, locally correlated positions that are locked in place. Although this limiting case cannot be literally realized in experiment, we shall show it is relevant to understanding the predictions of the full NMCT theory for high aspect ratios. Setting $r_{loc}=0$ in Eq. (39), the frozen CM-NMCT equation is

$$\theta_{loc}^{-2}=\frac{b^2}{12\pi^2}\exp(-\theta_{loc}^2/2)\int_0^\infty dq\rho q^4 C_{\rm CM}^2(q)S_{\rm CM}(q)\times[1-\sin(qb)/qb][1+\sin(qb)/qb]^{-3}\times\left\{\sum_{l=0}^{\infty} j_{2l}^2(qb/2)(4l+1)\exp[-l(2l+1)\theta_{loc}^2/2]\right\}^2. \quad (41)$$

The limiting vertex scaling with wave vector is again different. At small q, the vertex increases as $\sim q^6$, while it saturates (q independent) at high wave vectors.

IV. NUMERICAL PREDICTIONS OF NMCT

In this section, several NMCT predictions are worked out: the location and "order" (discontinuous versus continuous) of the ideal nonergodicity volume fractions for translation only (single localization, plastic glass) and simultaneous rotation and translation arrest (double-glass), CM localization length and rotational angle along, and beyond, the ideal glass lines, and the Debye-Waller factors. NMCT is a simplified formulation of the ideal mode coupling theory which addresses only the above properties and questions. Another goal of this section is to test the reliability of NMCT by comparing its predictions to those of the technically far more complex, but rigorous within the ideal MCT framework, "full" MCT results [11] for diatomics at the site level.

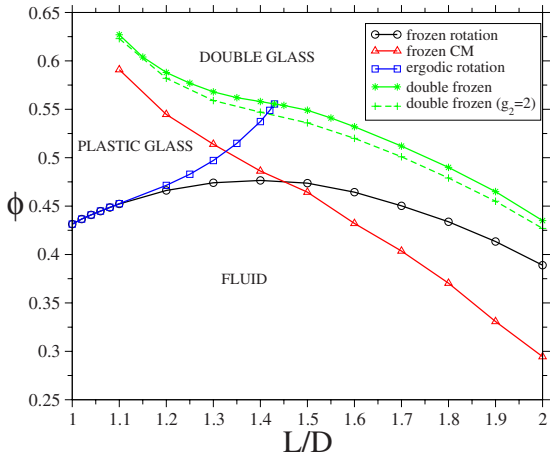

FIG. 1. (Color online) Nonergodicity boundaries predicted by NMCT in the volume fraction—aspect ratio representation. Five curves indicate CM nonergodicity boundary under the frozen rotation approximation (black circle), pure rotation nonergodicity boundary under frozen CM approximation (red triangle), fluid-plastic glass transition (blue square), double-glass transition (green solid star), and its analog with $g_2=2$ (green dashed plus). The intersection of the double-glass and fluid-plastic glass boundaries occurs at a triple point $L/D=1.43$.

A. Ideal nonergodicity phase diagram

Figure 1 shows the full NMCT nonergodicity boundaries determined from Eqs. (38) and (39). Ideal glass curves in the frozen rotation and frozen CM limits are also included. Three dynamical phases are predicted: fluid, plastic glass, and double glass. At low-enough volume fractions, only the trivial solution of Eqs. (38) and (39) exists, $r_{loc}=\infty$, $\theta_{loc}=\infty$, corresponding to ergodic translation and rotation. Upon increasing volume fraction, two types of nonergodicity transitions occur depending on aspect ratio. If $L/D<1.43$, a nontrivial solution of finite r_{loc} and infinite θ_{loc} emerges corresponding to the fluid-plastic glass transition at a volume fraction Φ_{fp}, i.e., the "ergodic rotation" limit of Eq. (40). Further increase of volume fraction leads to a double localization solution corresponding to the plastic glass–double-glass transition at a volume fraction Φ_{pd}. In contrast, if $L/D>1.43$, there is only one nonergodicity transition corresponding to simultaneous rotation and CM localization at a volume fraction Φ_{fd}. As $L/D\to 2$, the ideal glass transition volume fraction acquires a value very close to, but slightly above, that of hard spheres. The plastic glass and double-glass states merge in a cusplike fashion at a "triple point" at $L/D=1.43$ and $\Phi_t\simeq 0.56$. All nonergodicity transitions are "first order," i.e., discontinuous jumps of the dynamic order parameter(s).

The fluid-plastic glass line for $L/D<1.43$ and the fluid double-glass line for $L/D>1.43$, both represent a CM localization transition and constitute the *initial* nonergodicity boundary encountered as volume fraction is increased. Consistent with prior simplified CM-NMCT (frozen rotation) [18], this boundary is a nonmonotonic function of aspect ratio. Moreover, the hardest to vitrify state occurs at nearly the same value of $L/D\sim 1.43$ in both versions of NMCT.

The differences between the full and frozen rotation NMCT ideal glass boundaries are largest at intermediate aspect ratios. When the aspect ratio is relatively small, rotation has little effect and the full theory is virtually identical to its frozen rotation CM limit for $L/D<1.1$. For large aspect ratios, rotation is strongly constrained and the assumption it is frozen is a rather good approximation resulting in the full and CM version of NMCT glass boundaries approaching each other. As expected physically, the full theory always predicts higher volume fractions are required for kinetic arrest since rotational motion facilitates fluidity. Of course, rotation becomes more difficult at fixed volume fraction as the aspect ratio increases and hence the double-frozen glass curve in Fig. 1 is a monotonically decreasing function of aspect ratio.

Our overall conclusion is that the frozen rotation CM-NMCT [18] is qualitatively reliable for the restricted question of the location of the first ideal nonergodicity transition. However, this is not true of the other limiting case: the frozen CM glass boundary in Fig. 1. If the CM is pinned and the molecule can only rotate, then the volume fraction for orientational arrest decreases strongly with aspect ratio. For all aspect ratios, it lies below the double-frozen curve and undergoes curve crossing with the ergodic rotation and frozen rotation ideal glass boundaries.

The results in Fig. 1 also confirm our argument in Sec. II that the collective rotation factor, g_2, has a small quantitative influence on ideal glass boundaries. Double localization curves without ($g_2=1$) and with a fixed and rather large value ($g_2=2$) correction are close and the shapes of the double-glass arrest boundaries are qualitatively identical. In reality, g_2 depends on volume fraction and L/D in a potentially complex manner [38], but will not seriously modify the results.

The full site-site MCT [11] for hard diatomics also predicts three dynamical phases: fluid, plastic glass, and double glass. The initial nonergodicity boundary as spherical symmetry is broken is a discontinuous (type B) fluid-to-glass line in the full MCT, while the plastic glass to double-glass transition is continuous (type A). The latter is in contrast with NMCT which is based on just two scalar order parameters for which all dynamical transitions are discontinuous (type B). Quantitatively, the plastic glass–double-glass boundary in the full MCT is a nonmonotonic function of L/D which terminates in a cusplike manner at a triple point at the double-glass line at $L/D\sim1.34$. In detail, this differs from the results in Fig. 1 where the triple point is the maximum of the initial nonergodicity boundary. In full MCT, the latter occurs at $L/D\sim1.42$, in almost perfect agreement with NMCT. The ideal glass transition for $L/D=2$ is slightly higher than that for hard spheres in both the full MCT and NMCT. Quantitatively, the full MCT nonergodicity volume fractions are all higher compared to NMCT.

Finally, we note that if the crude Vineyard approximation for the collective Debye-Waller factor is used, the CM-NMCT kinetic arrest boundary is shifted down in volume fraction by ≈0.1 for all aspect ratios (not plotted). Hence, at the CM level, use of the more accurate de Gennes form of the collective DW factor results only in quantitative changes. However, for our NMCT that treats rotations and translations, qualitative changes occur which results in much poorer agreement between full MCT and our naïve formulation for the topology of the ideal kinetic arrest diagram [39].

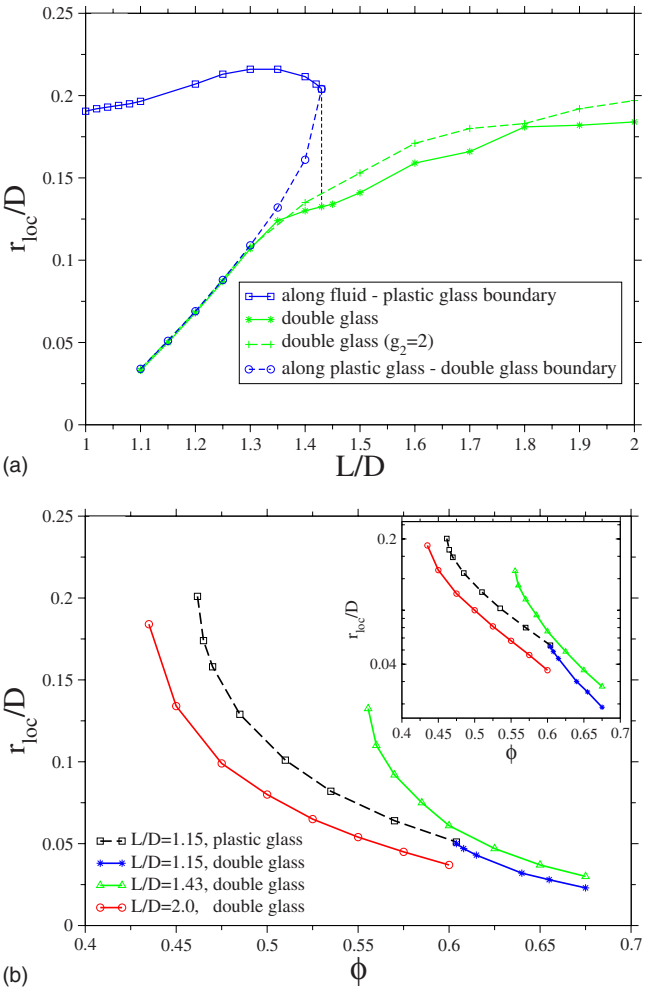

FIG. 2. (Color online) (a) CM localization length as a function of aspect ratio along the nonergodicity boundaries: fluid-plastic glass boundary (blue solid square), double-glass boundary (green solid star), double-glass boundary with $g_2=2$ (green dashed star), and plastic glass at the plastic glass–double-glass boundary (blue dashed circle). Black vertical dashed line indicates that at the triple point, r_{loc}/D discontinuously changes from 0.201 for the plastic glass to 0.133 for double-glass state. (b) Localization lengths as a function of volume fraction in the plastic glass or double-glass region for $L/D=1.15$, 1.43, and 2.0. Inset shows the same results in a log-linear format.

B. Localization length and angle

The center-of-mass localization lengths along the nonergodicity boundaries are shown in Fig. 2(a). For low aspect ratio diatomics, $r_{loc}/D\sim0.2$ at the plastic glass transition and is a weakly nonmonotonic function of aspect ratio. For $L/D<1.43$, at the plastic glass to double-glass transition, the CM localization length decreases discontinuously, which is most apparent at the triple point where r_{loc}/D changes from 0.201 to 0.133. The double-glass localization lengths based on $g_2=2$ are very close to the $g_2=1$ results. The NMCT

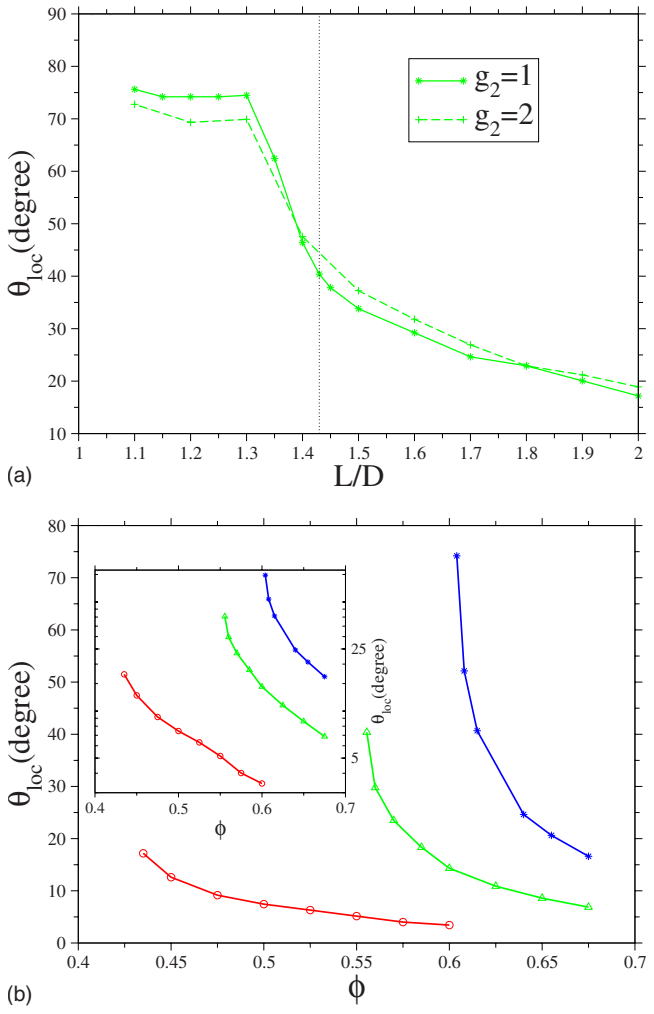

FIG. 3. (Color online) (a) Localization angle as a function of aspect ratio along the double-glass boundary: $g_2=1$ (solid star) and $g_2=2$ (dashed plus). The intersection of the green solid curve and the vertical dotted line indicates that at the triple point the localization angle discontinuously changes to infinity in plastic glass state. (b) Localization angles as a function of volume fraction in the double-glass region for $L/D=1.15$ (blue star), 1.43 (green triangle), and 2.0 (red circle). Inset is same results in a log-linear format.

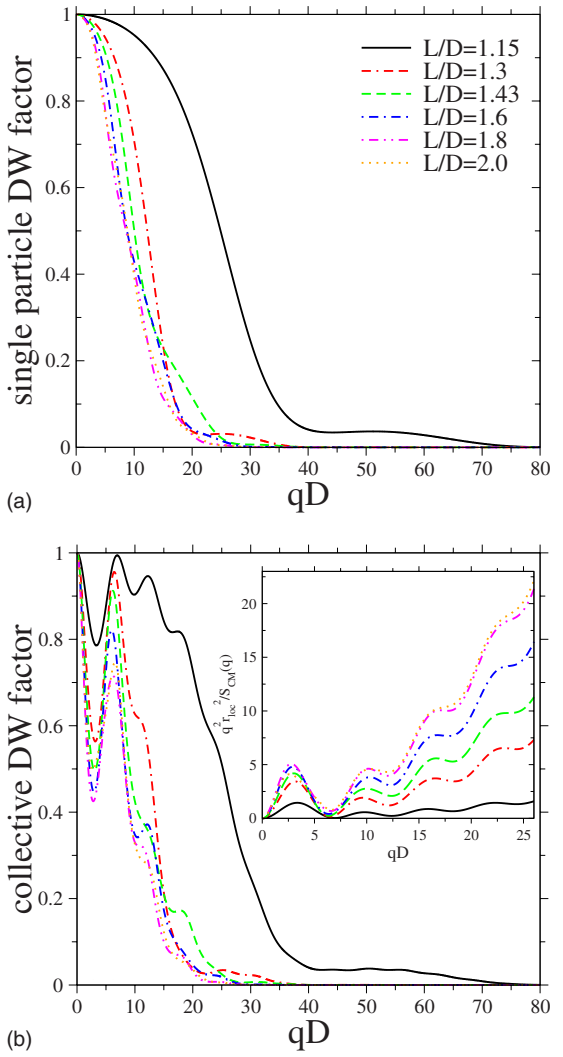

FIG. 4. (Color online) (a) Self-particle DW factors at the ideal double-glass boundary for $L/D=1.15$ (solid), 1.3 (dash-dot-dashed), 1.43 (dashed), 1.6 (dot-dashed), 1.8 (dot-dash-dotted), and 2.0 (dotted). (b) Analogous collective DW factors. Inset: argument of the collective DW factor as a function of wave vector.

predictions for the CM localization length along the first nonergodicity boundary are quite similar to those of full MCT [11], including the weakly nonmonotonic dependence on aspect ratio for small L/D and the sharp drop near the aspect ratio corresponding to the most difficult to vitrify state.

Along the double-glass line, r_{loc}/D monotonically increases with aspect ratio from ~0.03 at $L/D=1.1$ to ~0.18 at $L/D=2$. This trend is expected since the cage size must be smaller to constrain the rotational motion at higher volume fraction. In all cases, the CM localization lengths decrease with volume fraction above the nonergodicity boundaries as shown in Fig. 2(b) for three illustrative aspect ratios. The log-linear plot of the inset suggests a roughly exponential decay.

Figure 3 presents the analogous localization angle results. For all aspect ratios, θ_{loc} discontinuously jumps from infinity to the finite values as shown in Fig. 3(a). The localization angle along the double-frozen glass line is roughly a constant at ~75° for $L/D<1.3$. Beyond this aspect ratio, θ_{loc} decreases quickly and at the triple point $\theta_{loc}\sim 40°$, while for the largest aspect ratio is only ~15°. The localization angles predicted along the double-glass boundary based on $g_2=2$ are very close to the $g_2=1$ results. Figure 3(b) shows how the localization angles decrease with volume fraction above the double-frozen glass nonergodicity boundary; all θ_{loc} decrease to less than 20° at the highest volume fraction considered.

C. Debye-Waller nonergodicity factors

Figure 4 presents the self and collective Debye-Waller factors along the double-glass line for six aspect ratios. In the context of an ideal glass transition, these quantities are closely related to the intermediate time plateau behavior of dynamic structure factors. Due to partial rotational relax-

ation, the wave-vector dependence of the self-DW factors in Fig. 4(a) is not strictly Gaussian as true for hard spheres within NMCT. A two-step or plateaulike feature occurs at intermediate wave vector for modest aspect ratios. The shapes of the collective DW factors in Fig. 4(b) are similar to their self-counterparts but with additional oscillations that arise from the de Gennes narrowing correction factor in the CM Debye-Waller factor (see inset). Such oscillations are expected based on the full ideal MCT [11], but are absent if the collective DW factor of Eq. (34) is replaced by its Vineyard analog.

V. BEYOND MCT: DYNAMIC FREE-ENERGY LANDSCAPE AND ACTIVATED PROCESSES

A. Theory

The nonlinear Langevin equation approach that goes beyond MCT to treat single-particle activated barrier hopping was initially developed for spheres based on a heuristic, but physically motivated, generalization of NMCT [16,18]. Subsequently, it was derived from microscopic time-dependent statistical mechanics for one-component spherical particle fluids based on dynamic density-functional and local equilibrium ideas [40]. Recent applications to nonspherical particle fluids within the frozen rotation CM model exploited the direct analogy with spherical particles [18]. Most recently, the NMCT and NLE theories have been extended to treat "biphasic" mixtures composed of hard and sticky spheres [21] based on the heuristic route from NCMT to the NLE theory. This path is now adopted for the nonspherical particle fluid problem.

In the lightly space and time coarse-grained spirit of model A [41], the two coupled nonlinear Langevin stochastic equations of motion for the CM displacement and cumulative orientational angle displacement scalar dynamical variables are given in the overdamped (ignore inertia) limit as [16,21]

$$-\zeta_T \frac{d}{dt} r_{\mathrm{CM}} - \frac{\partial}{\partial r_{\mathrm{CM}}} F_{eff}(r_{\mathrm{CM}}, \theta) + \delta f_T = 0, \tag{42}$$

$$-\zeta_R \frac{d}{dt} \theta - \frac{\partial}{\partial \theta} F_{eff}(r_{\mathrm{CM}}, \theta) + \delta T_R = 0, \tag{43}$$

where the white-noise random force, δf_T, and random torque, δT_R, satisfy

$$\langle \delta f_T(0) \delta f_T(t) \rangle = 2 k_B T \zeta_T \delta(t), \tag{44}$$

$$\langle \delta T_R(0) \delta T_R(t) \rangle = 2 k_B T \zeta_R \delta(t), \tag{45}$$

$$\langle \delta f_T(0) \delta T_R(t) \rangle \equiv 0. \tag{46}$$

Here, ζ_T and ζ_R are short-time translational and rotational friction constants, respectively.

The use of a scalar CM displacement as the dynamic order parameter and isotropic equilibrium correlations to quantify caging constraints corresponds to the neglect of anisotropic CM motion associated with different mobilities parallel and perpendicular to the molecular axis. We follow the physically motivated heuristic approach originally proposed for spherical particle fluids and mixtures [16,21] to deduce the form of the dynamic free energy. In the long-time limit, the key NMCT quantities $\langle \vec{F}_{\mathrm{CM}}(0) \cdot \vec{F}_{\mathrm{CM}}(t) \rangle$ and $\langle \vec{T}(0) \cdot \vec{T}(t) \rangle$ obey equipartition relations which can be written as [21]

$$\beta \langle \vec{F}_{\mathrm{CM}}(0) \cdot \vec{F}_{\mathrm{CM}}(t \to \infty) \rangle r_{loc} - 3 k_B T / r_{loc} = \partial F_{eff}(r_{\mathrm{CM}}, \theta) / \partial r_{\mathrm{CM}}|_{r_{loc}, \theta_{loc}} = 0, \tag{47}$$

$$\beta \langle \vec{T}(0) \cdot \vec{T}(t \to \infty) \rangle \theta_{loc} - 2 k_B T / \theta_{loc} = \partial F_{eff}(r_{\mathrm{CM}}, \theta) / \partial \theta|_{r_{loc}, \theta_{loc}} = 0. \tag{48}$$

Based on the local equilibrium idea underlying the dynamical variable level density-functional approach [40], the ensemble-averaged localization length and angle that enter K_{CM} and K_{ROT} derived in Sec. II are then replaced by their instantaneous dynamical variable analogs thereby yielding

$$\frac{\beta \partial F_{ex}(r_{\mathrm{CM}}, \theta)}{\partial r_{\mathrm{CM}}} = \frac{2 r_{\mathrm{CM}}}{3 \pi^2} \int_0^\infty dq \rho q^4 C_{\mathrm{CM}}^2(q) S_{\mathrm{CM}}(q) [1 + \sin(qb)/qb]^{-2} \times \left\{ \sum_{l=0}^{\infty} j_{2l}^2(qb/2)(4l+1) \exp[-l(2l+1)\theta^2/2] \right\}^2 \times \exp\{-q^2 [1 + S_{\mathrm{CM}}^{-1}(q)] r_{\mathrm{CM}}^2 / 6\}, \tag{49}$$

$$\frac{\beta \partial F_{ex}(r_{\mathrm{CM}}, \theta)}{\partial \theta} = \frac{b^2 \theta}{6 \pi^2} \exp(-\theta^2/2) \int_0^\infty dq \rho q^4 C_{\mathrm{CM}}^2(q) S_{\mathrm{CM}}(q) \times [1 - \sin(qb)/qb][1 + \sin(qb)/qb]^{-3} \times \left\{ \sum_{l=0}^{\infty} j_{2l}^2(qb/2)(4l+1) \exp[-l(2l+1)\theta^2/2] \right\}^2 \times \exp\{-q^2 [1 + S_{\mathrm{CM}}^{-1}(q)] r_{\mathrm{CM}}^2 / 6\}, \tag{50}$$

where

$$\beta F_{eff} = -3 \ln r_{\mathrm{CM}} - 2 \ln \theta + \beta F_{ex}. \tag{51}$$

The two-dimensional dynamical free-energy surface follows via integration as

$$\beta F_{eff}(r_{\mathrm{CM}}, \theta) - \beta F_{eff}(r_{loc}, \theta_{loc}) = -3 \ln(r_{\mathrm{CM}}/r_{loc}) - 2 \ln(\theta/\theta_{loc}) + \int_{r_{loc}}^{r_{\mathrm{CM}}} dr' \frac{\beta \partial F_{ex}(r', \theta_{loc})}{\partial r'} + \int_{\theta_{loc}}^{\theta} d\theta' \frac{\beta \partial F_{ex}(r_{\mathrm{CM}}, \theta')}{\partial \theta'}. \tag{52}$$

By construction, the NLE theory of Eq. (49) reduces to ideal NMCT if the random thermal noise is ignored; a limit that effectively "turns off" activated barrier hopping [16,21,40].

As discussed in detail previously [40], the vertices in Eqs. (49) and (50) involve a mean-square effective force since dynamic density-functional ideas at the stochastic variable, not ensemble-averaged, level are the basis of the NLE approach.

In the ergodic rotation limit relevant for relatively small aspects ratios ($L/D<1.43$) at volume fractions below the double-glass boundary, the NLE theory reduces to one stochastic equation of motion for the CM described by a dynamical free energy given by

$$\beta F_{eff}(r_{\rm CM},\infty) = -3\ln(r_{\rm CM}) - \frac{32}{\pi^2}\int_0^\infty dq\rho q^2 C_{\rm CM}^2(q) S_{\rm CM}(q)\frac{\sin^4(qb/2)}{(qb)^4} \times\left[1+\frac{\sin(qb)}{qb}\right]^{-2}[1+S_{\rm CM}^{-1}(q)]^{-1} \times\exp\{-q^2[1+S_{\rm CM}^{-1}(q)]r_{\rm CM}^2/6\}. \quad (53)$$

For comparison, the effective free energy in the frozen rotation literal CM description is [18]

$$\beta F_{eff}(r_{\rm CM},0) = -3\ln(r_{\rm CM}) - \frac{1}{2\pi^2}\int_0^\infty dq\rho q^2 C_{\rm CM}^2(q) S_{\rm CM}(q) \times[1+S_{\rm CM}^{-1}(q)]^{-1}\exp\{-q^2[1+S_{\rm CM}^{-1}(q)]r_{\rm CM}^2/6\}. \quad (54)$$

The wave-vector dependence of the constraints encoded in the caging part of the dynamical free energy is different in Eqs. (53) and (54), with the localizing constraints stronger in Eq. (54).

B. Dynamic free-energy in the plastic glass phase

In the plastic glass region of the kinetic arrest diagram, Eqs. (53) and (54) can be compared. Figure 5 shows results for aspect ratios of 1.1, 1.2, and 1.3. The comparison is made at a common "distance from the ideal nonergodicity boundary," i.e., a fixed value of $\phi-\phi_c$. As expected, the barrier predicted by the frozen rotation CM model is larger and the localization length is slightly smaller than the new ergodic rotation limit results. Despite this generic difference, overall the dynamic free-energy curves determined by the two descriptions are qualitatively consistent.

C. Dynamic free-energy surfaces in the double-glass regime

The most interesting activated dynamics occurs in the double-glass region where the CM and rotational degrees of freedom are both temporally localized. The entropic barrier hopping process then occurs on a two-dimensional dynamic free-energy surface $F_{eff}(r_{\rm CM},\theta)$, results for which are shown in Fig. 6 for three representative aspect ratios of 1.15, 1.43, and 2.0. The volume fractions are chosen to be well above the double-frozen glass NMCT boundary in order to most clearly illustrate the cooperative nature of activated dynamical trajectories that determine the alpha relaxation process. In

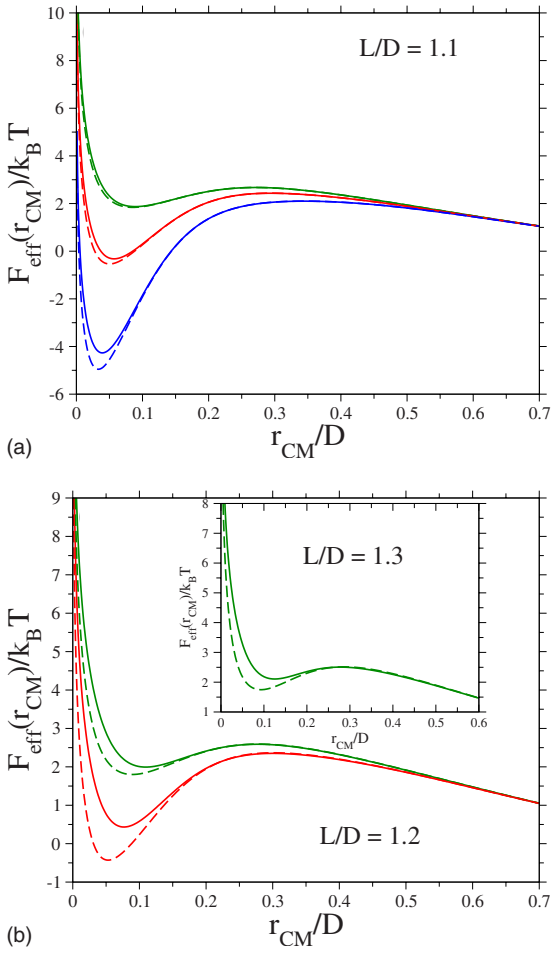

FIG. 5. (Color online) Dynamic free energy as a function of dimensionless CM displacement for the ergodic rotation limit of the full theory (solid curves) and the analogous CM mapping (frozen rotation; dashed curves) in the plastic glass region for aspect ratios of (a) 1.1, (from top to bottom) $\phi-\phi_c=0.05$, 0.1, and 0.15; (b) 1.2, (from top to bottom) $\phi-\phi_c=0.05$ and 0.1. Inset: $L/D=1.3$ and $\phi-\phi_c=0.05$.

all cases, the saddle-point trajectory (lowest entropic barrier) is associated with an aspect ratio and volume fraction dependent cooperative translation-rotation motion.

Figure 6(a) shows the dynamic free-energy surface for $L/D=1.15$ at $\phi=0.675$. Its qualitative form is characteristic of low aspect ratio systems which can exist in a plastic glass state. Specifically, relaxation will occur in a two-step activated manner. The lowest barrier to be surmounted is associated with mostly, but not entirely, rotational motion, i.e., a path almost parallel to the θ axis with the CM position nearly fixed at its localization point. One then expects partial rotational equilibration until random thermal noise ultimately drives at longer times hopping over the higher barrier associated with CM translation. Hence, a two-step activated process is predicted involving relatively low and high barriers corresponding to a partial separation of time scales.

As the aspect ratio grows, the form of the dynamic free-energy surface qualitatively changes. Examples are given in Fig. 6(b) ($L/D=1.43$, $\phi=0.65$) and Fig. 6(c) ($L/D=2.0$, $\phi=0.6$). A single saddle point now exists and a tra-

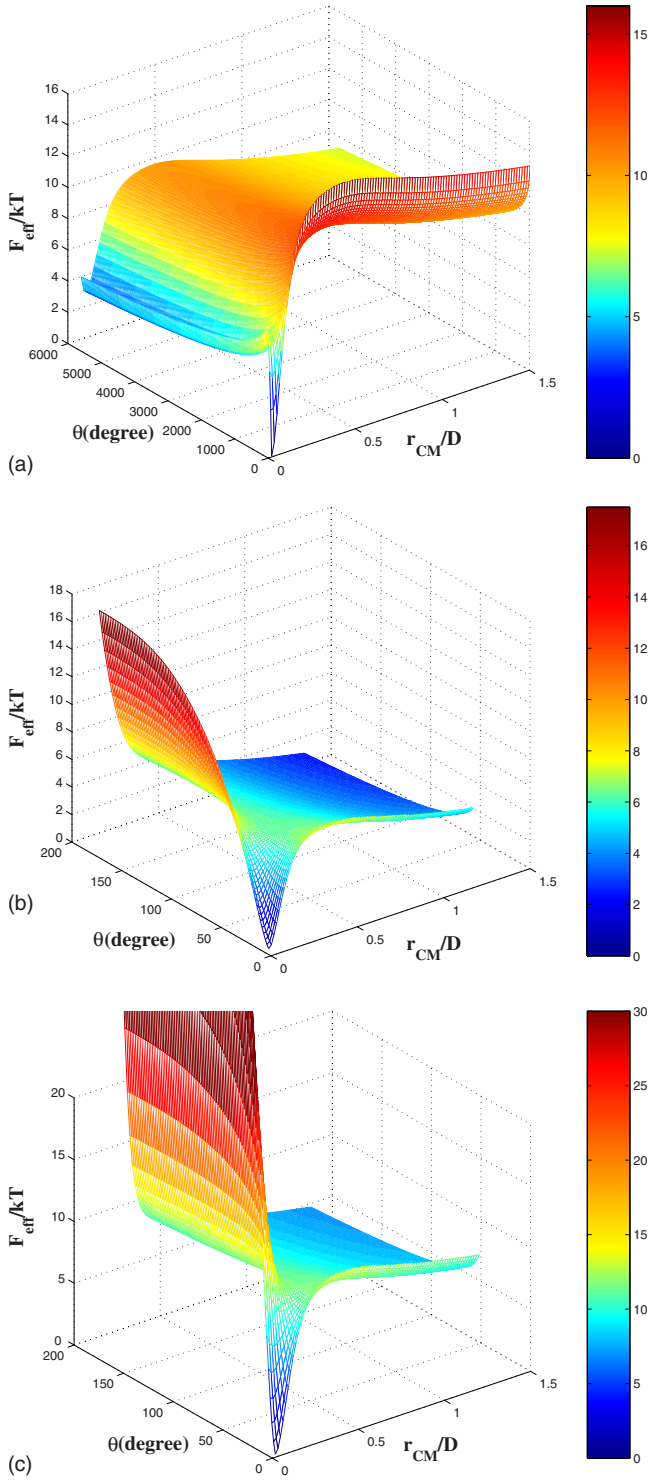

FIG. 6. (Color online) Dynamic free-energy surface as a function of CM translational displacement and rotational angle displacement for (a) $\phi=0.675$, $L/D=1.15$, (b) $\phi=0.65$, $L/D=1.43$, and (c) $\phi=0.6$, $L/D=2.0$ (note that the value of F_{eff}/kT as a function of r_{CM} and θ can be read off without the color bar).

jectory that follows this path involves substantial coupled translational and rotational displacements the precise mix of which depends on aspect ratio and volume fraction. One can anticipate the numerical solution of the coupled NLEs will result in a heterogeneous (since it is noise driven), but basically one step, relaxation process.

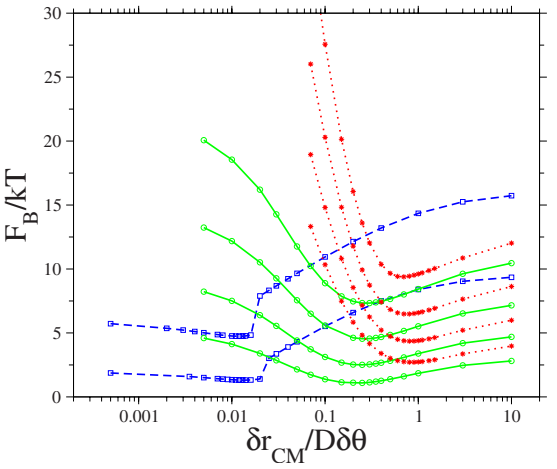

FIG. 7. (Color online) Entropic barrier height as a function of the direction of a trajectory on the two-dimensional free-energy surface as quantified by the ratio of CM and rotational (radians) displacements for $L/D=1.15$ (blue dashed square, from top to bottom, $\phi=0.675$ and 0.64), 1.43 (green solid circle, from top to bottom, $\phi=0.675$, 0.65, 0.625, and 0.6), and 2.0 (red dot star, from top to bottom, $\phi=0.6$, 0.575, 0.55, and 0.525).

Figure 7 summarizes the dynamic free-energy barrier heights as a function of the ratio of CM ($\delta r_{CM}=r_{CM}-r_{loc}$) to rotational ($\delta\theta=\theta-\theta_{loc}$) displacements for a range of volume fractions in the double-glass region. With increasing aspect ratio, more translational motion is involved in the activated hopping process, as indicated by a larger value of $\delta r_{CM}/D\delta\theta$ corresponding to the saddle-point (lowest barrier) trajectory. The shape of the curves in Fig. 7 becomes less shallow with increasing aspect ratio. This implies that the breadth of the relaxation-time distribution, and hence dynamic heterogeneity phenomena, will be strongly dependent on aspect ratio.

The qualitative beyond MCT results discussed above is consistent with the idea, previously suggested from computer simulation [13] and full MCT [11] studies, that at larger aspect ratios, CM translational and rotational motions are strongly coupled and the onset of slow glassy dynamics occurs at the same thermodynamic state point for translational and orientational motions. This is in contrast to low aspect ratio systems where a type of decoupling occurs which underlies the existence of the plastic glass state corresponding to translational motion being much slower than rotational motion. Recent simulations have suggested activated hopping processes are dominant for rotational dynamics at low aspect ratios and represent a channel for restoring ergodicity [13]. This observation is qualitatively consistent with our dynamical free-energy surface for $L/D=1.15$ and the proposed two-step (or two barriers, one low, one high) dynamical scenario. Most recently, simulations [14] of weakly anisotropic hard ellipsoids have found a two-step relaxation for various time correlations where the intermediate plateau can be very low. We suspect this behavior is also consistent with our theory (and the DW factors in Fig. 4), but definitive statements require numerical trajectory solution of the stochastic NLEs to compute ensemble-averaged time-correlation functions.

VI. SUMMARY AND FUTURE DIRECTIONS

The naïve MCT and nonlinear Langevin equation theories for the dynamical crossover and single-particle activated barrier hopping dynamics, respectively, have been generalized to treat the coupled translational and rotational dynamics of uniaxial objects in the glassy regime. The key idea that renders the generalization tractable is to introduce only two scalar dynamical variables: the displacement of the particle center-of-mass and orientational angle from their initial zero time values. Formulation of NMCT then requires the long-time limit of the autocorrelation of forces on a tagged particle center-of-mass and the corresponding torque quantity. NMCT predicts a kinetic arrest diagram with three phases: fluid, plastic glass, and double glass, the boundaries of which meet at a triple point corresponding to a most difficult to vitrify diatomic of aspect ratio ~1.43. The corresponding CM localization length and rotational angle have been computed along the ideal nonergodicity boundary and in the ideal arrested state. The relative roles of rotation and translation in determining the ideal kinetic arrest have been explored by examining three limiting approximations of the theory corresponding to the nonrotating model discussed previously [18], the frozen CM (pure rotation) model, and a rotationally ergodic model. Each of these limiting models captures the qualitative behavior of the full theory for specific ranges of aspect ratios.

The NMCT kinetic arrest boundaries represent the onset or crossover to activated barrier hopping dynamics. Two nonlinear Langevin equations have been proposed to describe the coupled translational and rotational dynamics of uniaxial particles. The fundamental quantity is a two-dimensional dynamic free-energy surface which quantifies effective forces on a particle CM and the corresponding torque. For small aspect ratio diatomics in the double-glass high volume fraction regime, the dynamic free-energy surface exhibits two saddle points reflecting a two-step activated dynamics where relatively rapid rotational dynamics coexists with slower CM translational motions. For large-enough aspect ratios, the dynamic free-energy surface has one saddle point which corresponds to an aspect ratio and volume fraction dependent coordinated translation-rotation motion. The entropic barriers as a function of the relative amount of rotation versus translation have been determined for several aspect ratios and volume fractions.

Much remains to be done, even for the simple diatomic system. The mean alpha or structural relaxation times for barrier crossing will be computed using multidimensional Kramers theory [21,42] as a systematic function of aspect ratio and volume fraction. From such information, crude estimates of a self-diffusion constant and rotational relaxation time can be obtained. More rigorously, stochastic Brownian trajectory solution of the coupled nonlinear Langevin equations can be performed which will deliver all single-particle time-correlation functions [17,18] and allow dynamical heterogeneity or non-Gaussian effects to be investigated [22].

The NMCT and NLE approaches formulated in this paper can be applied to several other problems of interest involving uniaxial objects. These include addressing the role of short-range attractions for homonuclear diatomics and the attendant phenomena of physical gelation and glass-fluid-gel reentrant transitions [2,20,43], steric asymmetry (heteronuclear diatomics), chemically patchy "Janus particles" corresponding to a large mismatch in intermolecular attraction between the two sites that compose the diatomic, and a probe diatomic in a hard-sphere solvent [44]. Work on these problems will be reported in future publications.

ACKNOWLEDGMENTS

This work was supported by the U.S. Department of Energy, Basic Energy Sciences via Grant No. DE-FG02-07ER46471 administered through the Frederick Seitz Materials Research Laboratory. We acknowledge stimulating conversations with C. F. Zukoski.

APPENDIX A: DERIVATION OF $\omega_{ss}(q,t)$

Consider the translation and rotation of a uniaxial Brownian object in solution in the absence of long-range hydrodynamic interactions [45]. Our goal is to compute the site-level intramolecular dynamic structure factors, $\omega_{ij}(q,t) = \langle e^{i\mathbf{q}\cdot[\mathbf{r}_i(t)-\mathbf{r}_j(0)]}\rangle$. The calculation can be performed based on the probability distribution function, $P(\mathbf{R}_{\mathrm{CM}},\mathbf{\Omega},t|\mathbf{0},\mathbf{\Omega}_0,0)$, that the CM is at $\mathbf{R}_{\mathrm{CM}}$ and molecular axis is at solid angle $\mathbf{\Omega}$ at time t, given the CM is at origin and the molecular axis is at solid angle $\mathbf{\Omega}_0$ at time zero. The simplest Fickian evolution equation is adopted

$$\frac{\partial}{\partial t}P(\mathbf{R}_{\mathrm{CM}},\mathbf{\Omega},t|\mathbf{0},\mathbf{\Omega}_0,0) = \left\{D_T\nabla_R^2 + \frac{D_R}{\sin^2\theta}\left[\sin\theta\frac{\partial}{\partial\theta}\left(\sin\theta\frac{\partial}{\partial\theta}\right)+\frac{\partial^2}{\partial\phi^2}\right]\right\} \times P(\mathbf{R}_{\mathrm{CM}},\mathbf{\Omega},t|\mathbf{0},\mathbf{\Omega}_0,0), \quad \text{(A1)}$$

where $P(\mathbf{R}_{\mathrm{CM}},\mathbf{\Omega},t=0|\mathbf{0},\mathbf{\Omega}_0,0)=\delta(\mathbf{R}_{\mathrm{CM}})\delta(\mathbf{\Omega}-\mathbf{\Omega}_0)$ and D_T and D_R are the translational and rotational diffusion coefficients, respectively. This is the Debye model [33,34] which describes rotational diffusion as a sequence of small scale random translational and orientational jumps. The solution of Eq. (A1) has the form [45] $P(\mathbf{R}_{\mathrm{CM}},\mathbf{\Omega},t|\mathbf{0},\mathbf{\Omega}_0,0) = p_T(\mathbf{R}_{\mathrm{CM}},t|\mathbf{0},0)p_R(\mathbf{\Omega},t|\mathbf{\Omega}_0,0)$, where

$$p_T(\mathbf{R}_{\mathrm{CM}},t|\mathbf{0},0) = \frac{1}{\sqrt{4\pi D_T t}}\exp(-R_{\mathrm{CM}}^2/4D_T t), \quad \text{(A2)}$$

$$p_R(\mathbf{\Omega},t|\mathbf{\Omega}_0,0) = \sum_{l=0}^{\infty}\sum_{m=-l}^{+l}\exp[-l(l+1)D_R t]Y_{lm}^*(\mathbf{\Omega}_0)Y_{lm}(\mathbf{\Omega}), \quad \text{(A3)}$$

and Y_{lm} is the spherical harmonic function. Now let $\mathbf{r}_i(t) = \mathbf{R}_{\mathrm{CM}}(t) + \mathbf{b}_i(t)$, where $\mathbf{b}_1(t) = b\vec{u}(t)/2$ and $\mathbf{b}_2(t) = -b\vec{u}(t)/2$, respectively. Using simple probability theory, one has

$$\omega_{ij}(q,t) = \frac{1}{4\pi}\int d\mathbf{R}_{\mathrm{CM}} \exp[i\mathbf{q}\cdot\mathbf{R}_{\mathrm{CM}}(t)] p_T(\mathbf{R}_{\mathrm{CM}},t|\mathbf{0},0) \times \int d\mathbf{\Omega}\int d\mathbf{\Omega}_0 \exp\{i\mathbf{q}\cdot[\mathbf{b}_i(t)-\mathbf{b}_j(0)]\} \times p_R(\mathbf{\Omega},t|\mathbf{\Omega}_0,0). \quad \text{(A4)}$$

The CM integration is straightforward to perform; to carry out the angular integration, the spherical wave expansion formula of a vector plane wave is employed

$$\exp(i\mathbf{a}\cdot\mathbf{c}) = \cos(\mathbf{a}\cdot\mathbf{c}) + i\sin(\mathbf{a}\cdot\mathbf{c}) = 4\pi\sum_{l=0}^{\infty}\sum_{m=-l}^{l} i^l j_l(ac) Y_{lm}^*(\mathbf{\Omega}_\mathbf{a}) Y_{lm}(\mathbf{\Omega}_\mathbf{c}), \quad \text{(A5)}$$

where $\mathbf{a}$ and $\mathbf{c}$ are two arbitrary vectors, $\mathbf{\Omega}_\mathbf{a}$ and $\mathbf{\Omega}_\mathbf{c}$ represent the solid angles along the two vectors, respectively, and the following two identities hold

$$\cos(\mathbf{a}\cdot\mathbf{c}) = 4\pi\sum_{l=even}\sum_{m=-l}^{l}(-1)^{l/2} j_l(ac) Y_{lm}^*(\mathbf{\Omega}_\mathbf{a}) Y_{lm}(\mathbf{\Omega}_\mathbf{c}), \quad \text{(A6)}$$

$$\sin(\mathbf{a}\cdot\mathbf{c}) = 4\pi\sum_{l=odd}\sum_{m=-l}^{l}(-1)^{(l-1)/2} j_l(ac) Y_{lm}^*(\mathbf{\Omega}_\mathbf{a}) Y_{lm}(\mathbf{\Omega}_\mathbf{c}). \quad \text{(A7)}$$

Substituting Eqs. (A2) and (A3) into Eq. (A4), one obtains

$$\omega_{11}(q,t) = \omega_{22}(q,t) = \frac{1}{4\pi}\exp(-q^2 D_T t)\int d\mathbf{\Omega}\int d\mathbf{\Omega}_0 \sum_{lm} Y_{lm}^*(\mathbf{\Omega}) Y_{lm}(\mathbf{\Omega}_0) \times \exp[-l(l+1)D_R t] \times \{\cos[(b/2)\mathbf{q}\cdot\vec{u}(\mathbf{\Omega})]\cos[(b/2)\mathbf{q}\cdot\vec{u}(\mathbf{\Omega}_0)] + \sin[(b/2)\mathbf{q}\cdot\vec{u}(\mathbf{\Omega})]\sin[(b/2)\mathbf{q}\cdot\vec{u}(\mathbf{\Omega}_0)]\}, \quad \text{(A8)}$$

$$\omega_{12}(q,t) = \omega_{21}(q,t) = \frac{1}{4\pi}\exp(-q^2 D_T t)\int d\mathbf{\Omega}\int d\mathbf{\Omega}_0 \sum_{lm} Y_{lm}^*(\mathbf{\Omega}) Y_{lm}(\mathbf{\Omega}_0) \times \exp[-l(l+1)D_R t] \times \{\cos[(b/2)\mathbf{q}\cdot\vec{u}(\mathbf{\Omega})]\cos[(b/2)\mathbf{q}\cdot\vec{u}(\mathbf{\Omega}_0)] - \sin[(b/2)\mathbf{q}\cdot\vec{u}(\mathbf{\Omega})]\sin[(b/2)\mathbf{q}\cdot\vec{u}(\mathbf{\Omega}_0)]\}. \quad \text{(A9)}$$

Utilizing Eqs. (A5)–(A7) and the identity

$$\sum_{m=-l}^{l}|Y_{lm}(\mathbf{\Omega}_\mathbf{q})|^2 = \frac{2l+1}{4\pi}, \quad \text{(A10)}$$

one finally obtains

$$\omega_{jj}(q,t) = \sum_{l=0}^{\infty} j_{2l}^2(qb/2)(4l+1)\exp\{-[q^2 D_T + 2l(2l+1)D_R]t\} + \sum_{l=0}^{\infty} j_{2l+1}^2(qb/2)(4l+3) \times \exp\{-[q^2 D_T + 2(2l+1)(l+1)D_R]t\}, \quad \text{(A11)}$$

$$\omega_{12}(q,t) = \omega_{21}(q,t) = \sum_{l=0}^{\infty} j_{2l}^2(qb/2)(4l+1) \times \exp\{-[q^2 D_T + 2l(2l+1)D_R]t\} - \sum_{l=0}^{\infty} j_{2l+1}^2(qb/2)(4l+3) \times \exp\{-[q^2 D_T + 2(2l+1)(l+1)D_R]t\}. \quad \text{(A12)}$$

The "dynamic site equivalency" approximation introduced in Sec. II B focuses on the total site-site dynamic intramolecular structure factor, $\omega_{ss}(q,t) = (1/2)\Sigma_{i,j}^2 \omega_{ij}(q,t)$. Using Eqs. (A11) and (A12) and performing the summation yield the desired result

$$\omega_{ss}(q,t) = 2\sum_{l=0}^{\infty} j_{2l}^2(qb/2)(4l+1) \times \exp\{-[q^2 D_T + 2l(2l+1)D_R]t\}. \quad \text{(A13)}$$

Finally, we note that our analysis based on Eq. (A1) ignores possible anisotropy of the CM motion of a uniaxial object included in the Smoluchowski-Perrin equation [46] corresponding to different CM diffusion constants parallel and perpendicular to the object axis. For the low-aspect ratio particles of present interest, this is a small effect since orientational motion is dominated by excluded volume interactions [14,36]. More generally, such anisotropy is averaged over by construction of our NLE theory which is based on the scalar absolute value of CM displacements and the quantification of dynamical caging constraints via ensemble-averaged, isotropic site-site equilibrium correlations [40].

APPENDIX B: VERTICES AND NAÏVE MODE COUPLING THEORY INTEGRANDS

MCT includes the consequences of force fluctuation on all length scales via an integration over wave vector in Eqs. (38) and (39), the integrand of which consists of two multiplicative parts: (i) a "vertex" defined as the full integrand if the

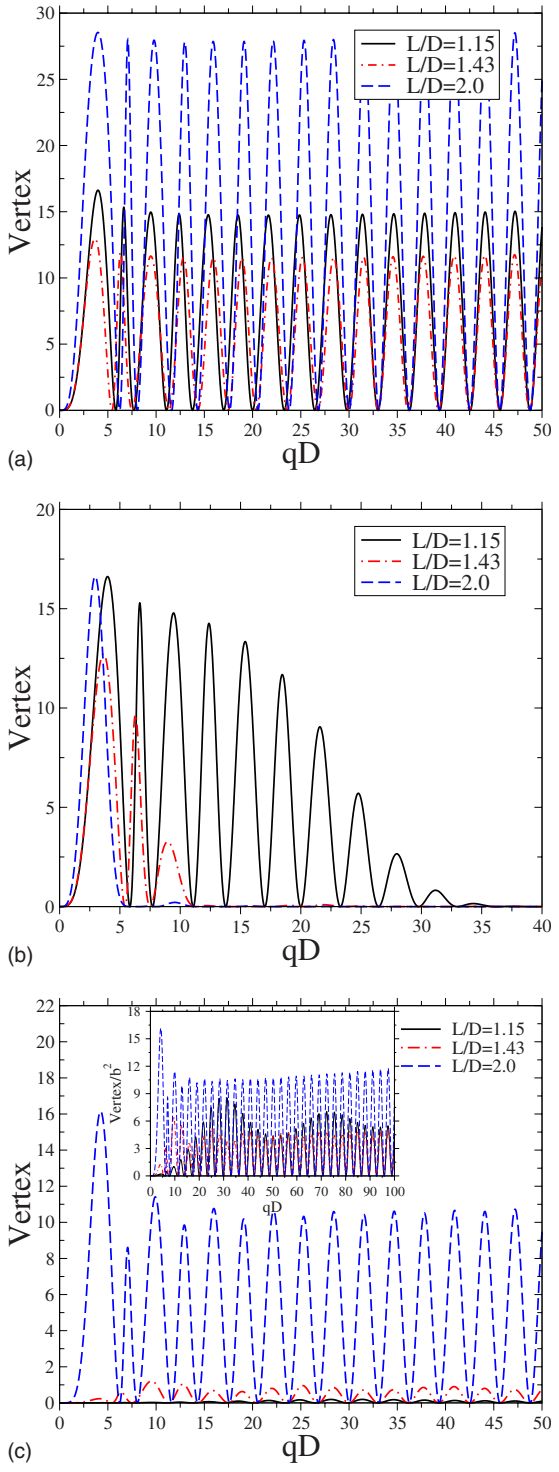

FIG. 8. (Color online) Vertex calculations for $L/D=1.15$ (solid), 1.43 (dot-dashed), and 2.0 (dashed) at a fixed volume fraction of 0.5 for (a) force vertex and frozen rotation, (b) force vertex and ergodic rotation, and (c) torque vertex and frozen CM. Inset: same results rescaled by the bond length squared.

DW factors are set equal to unity ($r_{loc}=\theta_{loc}=0$) and (ii) the DW factors. If the DW factors are included, we refer to the integrand as its "full" force (for CM displacement) or torque (for rotational displacement) value. The goal of this appendix

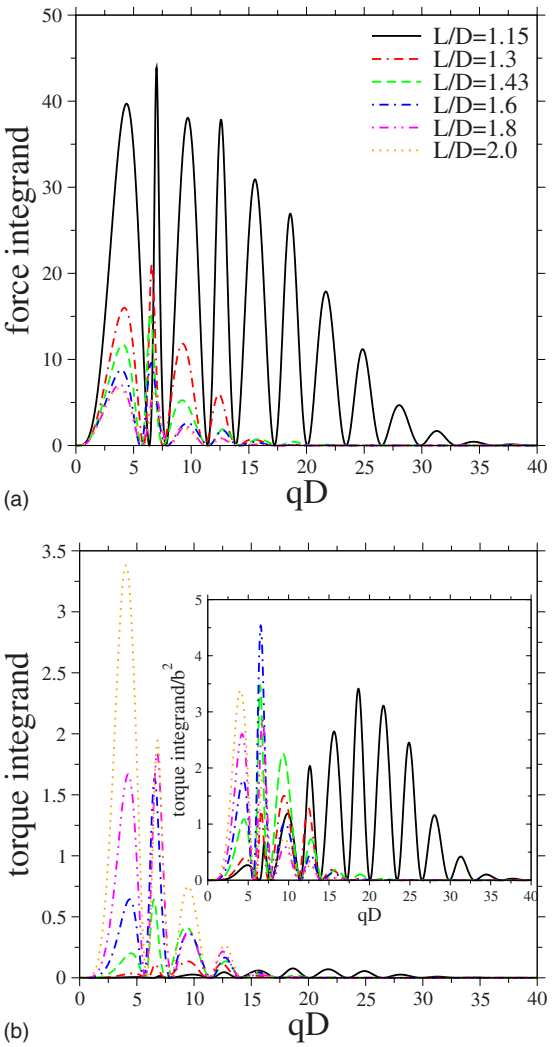

FIG. 9. (Color online) Integrand calculations for aspect ratios of 1.15 (solid), 1.3 (dash-dot-dashed), 1.43 (dashed), 1.6 (dot-dashed), 1.8 (dot-dash-dotted), and 2.0 (dotted) along the double-frozen glass boundary for (a) force integrand and (b) torque integrand. Inset: same results rescaled by the bond length squared.

is to gain insight as to what wave vectors are dominant in the vertices and full integrands.

We first rewrite Eqs. (38) and (39) as

$$\frac{1}{3}\beta^2\langle \mathbf{F}_{\mathrm{CM}}(0)\cdot\mathbf{F}_{\mathrm{CM}}(\infty)\rangle$$

$$= \frac{2}{9\pi^2}\int_0^\infty dq\rho q^4 C_{\mathrm{CM}}^2(q)S_{\mathrm{CM}}(q)[1+\sin(qb)/qb]^{-2} \times\exp\{-q^2[1+S_{\mathrm{CM}}^{-1}(q)]r_{loc}^2/6\} \times\left\{\sum_{l=0}^{\infty} j_{2l}^2(qb/2)(4l+1)\exp[-l(2l+1)\theta_{loc}^2/2]\right\}^2$$

$$= r_{loc}^{-2} = \int_0^\infty dq(\text{force integrand}), \qquad \text{(B1)}$$

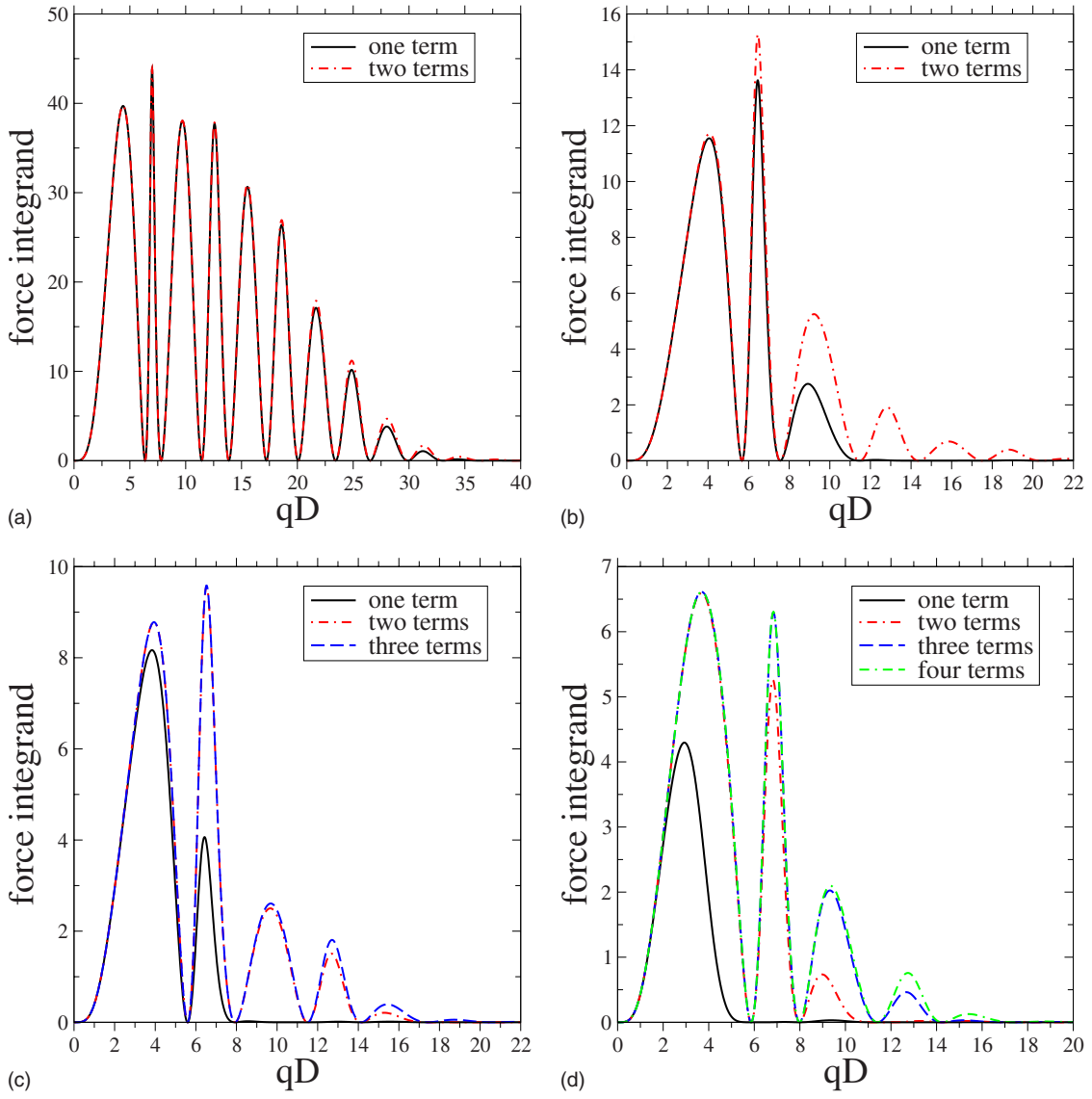

FIG. 10. (Color online) Convergence of the force integrand as a function of the number of angular-momentum contributions (l terms as indicated) at double-glass line for (a) $L/D=1.15$, (b) $L/D=1.43$, (c) $L/D=1.6$, and (d) $L/D=2.0$.

$$\frac{1}{2}\beta^2\langle\vec{T}(0)\cdot\vec{T}(\infty)\rangle$$
$$= \frac{b^2}{12\pi^2}\exp(-\theta_{loc}^2/2)\int_0^\infty dq\rho q^4 C_{\mathrm{CM}}^2(q)S_{\mathrm{CM}}(q)$$
$$\times[1-\sin(qb)/qb][1+\sin(qb)/qb]^{-3}$$
$$\times\exp\{-q^2[1+S_{\mathrm{CM}}^{-1}(q)]r_{loc}^2/6\}$$
$$\times\left\{\sum_{l=0}^{\infty} j_{2l}^2(qb/2)(4l+1)\exp[-l(2l+1)\theta_{loc}^2/2]\right\}^2$$
$$= \theta_{loc}^{-2} = \int_0^\infty dq(\text{torque integrand}). \quad \text{(B2)}$$

There are three types of vertices for the force and torque integrands. Substituting $r_{loc}=0$ and $\theta_{loc}=0$ into Eq. (B1), the *force vertex function of frozen rotation* is

$$\text{vertex}(q) = \frac{1}{18\pi^2}\rho q^4 C_{\mathrm{CM}}^2(q)S_{\mathrm{CM}}(q), \quad \text{(B3)}$$

which quantifies the Fourier-resolved effective mean-square force on the CM with frozen rotation. Substituting $r_{loc}=0$ and $\theta_{loc}=\infty$ into Eq. (B1), the *force vertex function of ergodic rotation* is,

$$\text{vertex}(q) = \frac{32}{9\pi^2}\rho C_{\mathrm{CM}}^2(q)S_{\mathrm{CM}}(q)\frac{\sin^4(qb/2)}{b^4}\left[1+\frac{\sin(qb)}{qb}\right]^{-2}. \quad \text{(B4)}$$

Substituting $r_{loc}=0$ and $\theta_{loc}=0$ into Eq. (B2) yields the *torque vertex function of frozen* CM,

$$\text{vertex}(q) = \frac{b^2}{48\pi^2} q^4 \rho C_{\text{CM}}^2(q) S_{\text{CM}}(q) \left[1 - \frac{\sin(qb)}{qb} \right] \times \left[1 + \frac{\sin(qb)}{qb} \right]^{-1}. \quad \text{(B5)}$$

We now numerically compare vertex functions for diatomics of three aspect ratios $L/D=1.15$, 1.43, and 2.0 at a fixed volume fraction of $\phi=0.5$. In Fig. 8(a), force vertex functions in the frozen rotation limit (CM-NMCT [18]) are shown. As previously demonstrated and theoretically understood [26], the generic behavior is an essentially constant amplitude, which is a nonmonotonic function of L/D, for wave vectors beyond the first two oscillations. For $L/D=1.43$, the amplitude is the smallest. This nonmonotonic behavior of the force vertex is consistent with the nonmonotonic CM frozen line (black circle curve in Fig. 1) described by Eq. (25).

In Fig. 8(b), the force vertex functions in the ergodic rotation limit (relevant to the plastic glass phase) are compared. For all aspect ratios, the vertex vanishes at large wave vectors and more rapidly with increasing aspect ratio. This is consistent with the monotonically increasing ergodic rotation ideal glass boundary (blue curve) in Fig. 1. For the largest aspect ratio $L/D=2$, the vertex vanishes after just one oscillation. Hence, the force vertex functions of frozen rotation and ergodic rotation are qualitatively different. The former is dominated by the largest wave vectors, while the latter is dominated by smaller wave vectors.

In Fig. 8(c), the torque vertex functions for the frozen CM limit model are shown. The amplitude is also nonzero in the large wave vector limit. A new feature (revealed in the inset) is an additional oscillation with wave length $\sim 2\pi/b$, which arises from the $\sin(qb)$ factor in Eq. (B5). The magnitude of the vertex monotonically increases with aspect ratio, consistent with the monotonic frozen CM glass boundary (red triangle curve in Fig. 1).

The force and torque integrands must vanish at large wave vectors due to the DW factors. Hence, the integrands are dominated by wave vectors of order the inverse of the CM localization length or characteristic q value of decay of the square of $j_{2l}(qb)$. To estimate the effective cutoff wave vector for the integration in Eqs. (B1) and (B2), we present the force integrand [Fig. 9(a)] and torque integrand [Fig. 9(b)] for $L/D=1.15$, 1.3, 1.43, 1.6, 1.8, and 2.0 along the double-frozen glass line (Fig. 1). Both integrands decay at a rate that increases with aspect ratio. For the slowest decaying case of $L/D=1.15$, the integrands vanish beyond $qD\sim 40$.

Finally, there is the question of how many "angular-momentum" terms in the infinite series $\Sigma_{l=0}^{\infty} j_{2l}^2(qb/2)(4l+1)\exp[-l(2l+1)\theta_{loc}^2/2]$ are required to achieve the converged numerical results. Figure 10 shows that the answer depends on aspect ratio where results for $L/D=1.15$, 1.43, 1.6, and 2.0 are presented along the double-frozen glass nonergodicity boundary. The notation "one term" indicates that only the $l=0$ contribution is included in the calculation, "two terms" indicates only $l=0$ and $l=1$ contributions are included, etc. In all cases, the convergence is fast. For $L/D=1.15$ and 1.43, only two l terms are needed to produce accurate results. Even for the system which needs the most angular-momentum states ($L/D=2$), four terms produce nearly the exact infinite series result. The reason that more terms are required for convergence at larger aspect ratios is that the localization angle is generally smaller and hence the l-dependent exponential in the infinite series decrease more slowly.

[1] See, for example, K. L. Ngai J. Non-Cryst. Solids **275**, 7 (2000); C. A. Angell, K. L. Ngai, G. B. McKenna, P. F. McMillan, and S. W. Martin, J. Appl. Phys. **88**, 3113 (2000); J. C. Dyre, Rev. Mod. Phys. **78**, 953 (2006).

[2] W. C. K. Poon, J. Phys.: Condens. Matter **14**, R859 (2002).

[3] G. J. Vroege and H. N. W. Lekkerkerker, Rep. Prog. Phys. **55**, 1241 (1992).

[4] D. Thies-Weesie, A. P. Philipse, and S. Kluijtmans, J. Colloid Interface Sci. **174**, 211 (1995); J. Buitenhius and A. P. Philipse, *ibid.* **176**, 272 (1995); J. Wijnhoven, D. van't Zand, D. van der Beek, and H. N. W. Lekkerkerker, Langmuir **21**, 10422 (2005).

[5] For reviews, see S. C. Glotzer and M. J. Solomon, Nature Mater. **6**, 557 (2007); A. van Blaaderen, Nature (London) **439**, 545 (2006); S. C. Glotzer, M. J. Solomon, and N. A. Kotov, AIChE J. **50**, 2978 (2004).

[6] V. N. Manoharan, M. T. Elseser, and D. J. Pine, Science **301**, 483 (2003).

[7] See, for example, E. B. Mock, H. De Bruyn, B. S. Hawkett, R. G. Gilbert, and C. F. Zukoski, Langmuir **22**, 4037 (2006); P. M. Johnson, C. M. van Kats, and A. van Blaaderen, *ibid.* **21**, 11510 (2005); T. Sun and Y. Xia, Science **298**, 2176 (2002).

[8] W. Götze, *Liquids, Freezing and the Glass Transition* (North-Holland, Amsterdam, 1991); W. Götze and L. Sjörgen, Rep. Prog. Phys. **55**, 241 (1992).

[9] S. Das, Rev. Mod. Phys. **76**, 785 (2004).

[10] R. Schilling, Phys. Rev. E **65**, 051206 (2002); C. Theis, F. Sciortino, A. Latz, R. Schilling, and P. Tartaglia, *ibid.* **62**, 1856 (2000); M. Letz, R. Schilling, and A. Latz, *ibid.* **62**, 5173 (2000).

[11] S.-H. Chong, and W. Götze, Phys. Rev. E **65**, 041503 (2002); **65**, 051201 (2002).

[12] Th. Theenhaus, M. P. Allen, M. Letz, A. Latz, and R. Schilling, Eur. Phys. J. E **8**, 269 (2002).

[13] A. J. Moreno, S.-H. Chong, W. Kob, and F. Sciortino, J. Chem. Phys. **123**, 204505 (2005); S.-H. Chong, A. J. Moreno, F. Sciortino, and W. Kob, Phys. Rev. Lett. **94**, 215701 (2005).

[14] P. Pfleiderer, K. Milinkovic, and T. Schilling, Europhys. Lett. **84**, 16003 (2008).

[15] S. H. Chong and W. Kob, Phys. Rev. Lett. **102**, 025702 (2009).

[16] K. S. Schweizer and E. J. Saltzman, J. Chem. Phys. **119**, 1181 (2003); E. J. Saltzman and K. S. Schweizer, *ibid.* **119**, 1197 (2003).

[17] E. J. Saltzman and K. S. Schweizer, J. Chem. Phys. **125**, 044509 (2006); Phys. Rev. E **74**, 061501 (2006); **77**, 051504 (2008).
[18] G. Yatsenko and K. S. Schweizer, J. Chem. Phys. **126**, 014505 (2007); Phys. Rev. E **76**, 041506 (2007); Langmuir **24**, 7474 (2008).
[19] T. R. Kirkpatrick and P. G. Wolynes, Phys. Rev. A **35**, 3072 (1987).
[20] Y. L. Chen and K. S. Schweizer, J. Chem. Phys. **120**, 7212 (2004); Y. L. Chen, V. Kobelev, and K. S. Schweizer, Phys. Rev. E **71**, 041405 (2005).
[21] D. C. Viehman and K. S. Schweizer, J. Chem. Phys. **128**, 084509 (2008); Phys. Rev. E **78**, 051404 (2008).
[22] K. S. Schweizer, Curr. Opin. Colloid Interface Sci. **12**, 297 (2007).
[23] Y. Brumer and D. R. Reichman, Phys. Rev. E **69**, 041202 (2004).
[24] A. Donev, I. Cisse, D. Sachs, E. A. Variano, F. H. Stillinger, R. Connelly, S. Torquato, and P. M. Chaikin, Science **303**, 990 (2004).
[25] S. R. Williams and A. P. Philipse, Phys. Rev. E **67**, 051301 (2003).
[26] K. S. Schweizer and G. Yatsenko, J. Chem. Phys. **127**, 164505 (2007); K. S. Schweizer, *ibid.* **127**, 164506 (2007).
[27] D. Chandler and H. C. Andersen, J. Chem. Phys. **57**, 1930 (1972).
[28] D. Chandler, in *Studies in Statistical Mechanics*, edited by J. L. Lebowitz and E. W. Montroll (North Holland, Amsterdam, 1982), Vol. 8, p. 275.
[29] I. Pagonabarraga and M. E. Cates, Europhys. Lett. **55**, 348 (2001).
[30] J.-P. Hansen and I. R. McDonald, *Theory of Simple Liquids*, 3rd ed. (Academic Press, New York, 2006.
[31] M. Benmouna, H. Benoit, M. Duval, and Z. Akcasu, Macromolecules **20**, 1107 (1987).
[32] M. R. Harpham, B. M. Ladanyi, N. E. Levinger, and K. W. Herwig, J. Chem. Phys. **121**, 7855 (2004).
[33] P. Debye, *Polar Molecules* (Dover, New York, 1929).
[34] T. G. Lombardo, F. H. Stillinger, and P. G. Debenedetti, J. Chem. Phys. **125**, 174507 (2006).
[35] M. G. Mazza, N. Giovambattista, F. W. Starr, and H. E. Stanley, Phys. Rev. Lett. **96**, 057803 (2006).
[36] S. Kammerer, W. Kob, and R. Schilling, Phys. Rev. E **56**, 5450 (1997).
[37] P. G. Wolynes and J. M. Deutch, J. Chem. Phys. **67**, 733 (1977).
[38] D. M. Richardson and D. Chandler, J. Chem. Phys. **80**, 4484 (1984), and references cited therein.
[39] Use of the crude Vineyard approximation for the collective Debye Waller factor still results in the NMCT prediction of three dynamic phases. The shape of the plastic glass to double-glass boundary is qualitatively identical to its de Gennes narrowing based analog in Fig. 1. However, the dynamic triple point is destroyed, in strong disagreement with the most accurate version of NMCT and also the full ideal MCT [11].
[40] K. S. Schweizer, J. Chem. Phys. **123**, 244501 (2005).
[41] N. Goldenfeld, *Lectures on Phase Transitions and the Renormalization Group* (Addison-Wesley, Reading, MA, 1992).
[42] J. S. Langer, Ann. Phys. **54**, 258 (1969).
[43] E. Zaccarelli, J. Phys.: Condens. Matter **19**, 323101 (2007); J. Bergenholtz and M. Fuchs, Phys. Rev. E **59**, 5706 (1999); J. Bergenholtz, W. Poon, and M. Fuchs, Langmuir **19**, 4493 (2003); K. Dawson, G. Foffi, M. Fuchs, W. Götze, F. Sciortino, M. Sperl, P. Tartaglia, T. Voigtmann, and E. Zaccarelli, Phys. Rev. E **63**, 011401 (2000).
[44] S. H. Chong, W. Gotze, and A. P. Singh, Phys. Rev. E **63**, 011206 (2000).
[45] B. J. Berne and R. Pecora, *Dynamic Light Scattering: With Applications to Chemistry, Biology, and Physics* (Dover, New York, 2000).
[46] T. Munk, F. Höflng, E. Fery, and T. Franosch, Europhys. Lett. **85**, 30003 (2009).